Crustal segmentation, composite looping pressure-temperature paths, and magma-enhanced metamorphic field gradients: Upper Granite Gorge, Grand Canyon, USA

Gregory Dumond†
Kevin H. Mahan‡
Michael L. Williams
Department of Geosciences, University of Massachusetts, Amherst, Massachusetts 01003, USA

Karl E. Karlstrom
Department of Earth and Planetary Sciences, University of New Mexico, Albuquerque, New Mexico 87131, USA

ABSTRACT

The Paleoproterozoic orogen of the southwestern United States is characterized by a segmented, block-type architecture consisting of tens of kilometer-scale blocks of relatively homogeneous deformation and metamorphism bounded by subvertical high-strain zones. New field, microstructural, and petrologic observations combined with previously published structural and geochronological data are most consistent with a tectonometamorphic history characterized by a clockwise, looping pressure-temperature (*P-T*) path involving: (1) initial deposition of volcanogenic and turbiditic supracrustal rocks at ca. 1.75–1.74 Ga, (2) passage from <12 km (below pressures equivalent to the aluminosilicate triple point) to ~25 km depths (~0.7 GPa) between ca. 1.70 and 1.69 Ga, (3) decompression back to ~12 km depths (0.3–0.4 GPa) by ca. 1.68 Ga, and (4) a protracted period of near-isobaric cooling (ca. 200–250 Ma). The general geometry of this looping *P-T* path is similar for rocks across the entire traverse; however, significant differences in peak temperatures are recorded (~500 to >750 °C). Notable variations along the transect are also primarily thermal in nature and include differences in the temperature of the prograde history (i.e., early andalusite versus kyanite), equilibrium pressures recorded at peak temperatures, and intensity of late-stage thermal spikes due to local dike emplacement. High-precision Δ*PT* "relative" thermobarometry confirms lateral temperature variations on the order of 100–250 °C with little to no variation in pressure. The Upper Granite Gorge thus represents a subhorizontal section of lowermost middle continental crust (~0.7 GPa). Results imply that the entire ~70-km-long transect decompressed from ~0.7 to ~0.3–0.4 GPa levels as one large coherent block in the Paleoproterozoic.

The transect represents a 100% exposed field laboratory for understanding the heterogeneity and rheologic behavior of lowermost middle continental crust during orogenesis. Hot blocks achieved partial melting conditions during penetrative subvertical fabric development. Although these blocks were weak, large-scale horizontal channel flow was apparently inhibited by colder, stronger blocks that reinforced and helped preserve the block-type architecture. Development of dramatic lateral thermal gradients and discontinuities without breaks in crustal level is attributed to: (1) spatially heterogeneous advective heat flow delivered by dense granitic pegmatite dike complexes and (2) local transcurrent displacements along block-bounding high-strain zones over an ~15–20 m.y. time interval. Exhumation of the transect from 25 to 12 km depths is interpreted to reflect erosion synchronous with penetrative development of steeply dipping NE-striking foliations and steeply plunging stretching lineations, consistent with an orogen-scale strain field involving NW-SE subhorizontal shortening and subvertical extension during crustal thickening.

Keywords: Grand Canyon, *P-T-t-D* path, continental crust, rheology, channel flow.

INTRODUCTION

Proterozoic rocks of southwestern North America are part of a >1000-km-wide orogenic belt that records the progressive southward growth of Laurentia (Karlstrom et al., 2001) (Fig. 1). An enigmatic characteristic of the belt is its block-type architecture, i.e., blocks with internally homogeneous deformational and metamorphic characteristics are separated by subvertical high-strain zones from blocks with different characteristics (Karlstrom and Bowring, 1988). This distinctive architecture has been investigated for over twenty-five years, with particular focus on issues involving growth, stabilization, reactivation, and the general character of middle continental crust (Karlstrom and Williams, 2006). Consequently, there is now great potential for use of this natural field laboratory to answer first-order questions about middle to lower crustal processes. In particular, to what extent does the block-type architecture reflect the original accretionary geometry of the orogen as opposed to the result of subsequent upper to middle crustal tectonism? How susceptible is the middle continental crust to flow as a channel during orogenesis (e.g., Beaumont et al., 2004)? And, how does rheology of continental crust evolve through time (e.g., Klepeis et al., 2004)? The answers to these questions have important implications for our understanding of the evolving strength and behavior of continental crust

†Corresponding author e-mail: gdumond@geo.umass.edu.
‡Current address: Mail Stop 100-23, Division of Geological and Planetary Sciences, California Institute of Technology, Pasadena, California 91125, USA.

GSA Bulletin; January/February 2007; v. 119; no. 1/2; p. 202–220; doi: 10.1130/B25903.1; 12 figures; Data Repository item 2007007.

For permission to copy, contact editing@geosociety.org
© 2006 Geological Society of America

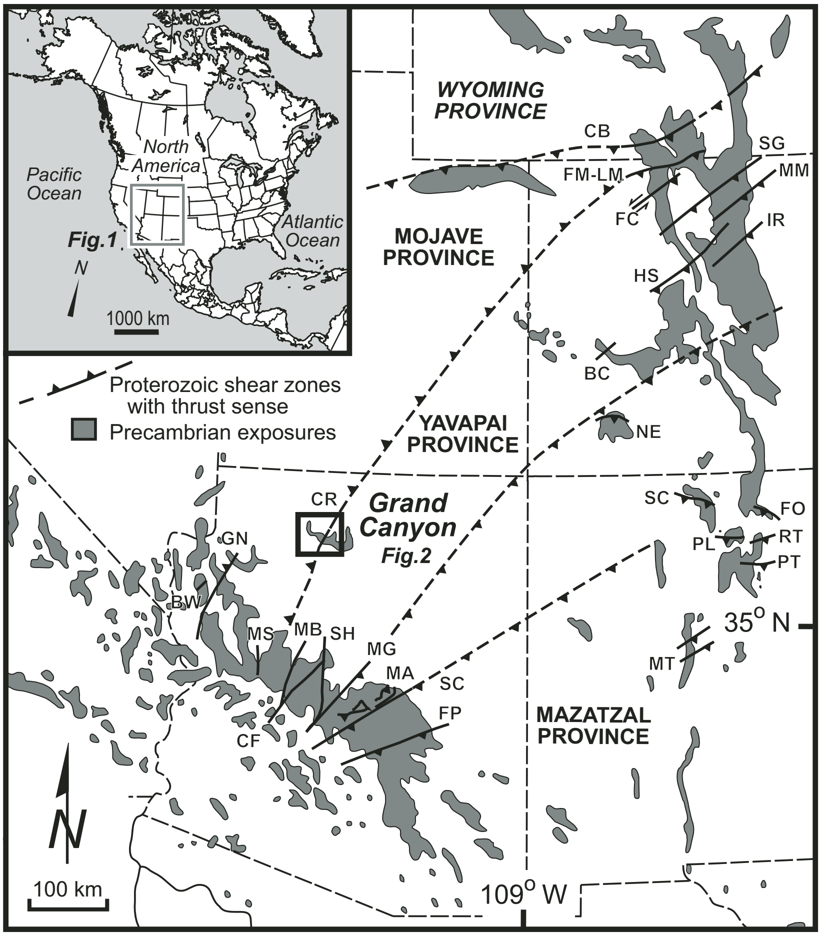

Figure 1. Map of exposed Proterozoic rocks in southwestern Unites States with major provinces and shear zones and location of Grand Canyon (modified after Karlstrom and Williams, 2006). CB—Cheyenne belt; FM-LM—Farwell Mountain–Lester Mountain shear zone; SG—Skin Gulch shear zone; FC—Fish Creek–Soda Creek shear zone; MM—Moose Mountain shear zone; IR—Idaho Springs–Ralston shear zone; HS—Homestake shear zone; BCG—Black Canyon; NE—Needle Mountains; BW—Big Wash shear zone; GN—Gneiss Canyon shear zone; CR—Crystal shear zone; MS—Mountain Spring shear zone; MB—Mesa Butte fault; CF—Chaparral fault; SH—Shylock shear zone; MG—Moore Gulch fault; MA—Mazatzal thrust belt; SC—Slate Creek shear zone; FP—Four Peaks shear zone; SP—Spring Creek shear zone; FO—Fowler Pass shear zone; PL—Plomo thrust; RT—Rincon thrust belt; PT—Pecos thrust; MT—Manzano thrust belt.

during orogenesis and the subsequent stabilization and preservation of continental lithosphere.

Field transects of tilted crustal sections or large exposures of exhumed middle to lower continental crust represent important laboratories for understanding the character and evolution of deformation, magmatism, and metamorphism at different crustal levels (e.g., Proterozoic rocks of northern New Mexico: Grambling, 1986; the Kapuskasing Uplift: Percival and West, 1994; the Fiordland-Westland orogen: Klepeis et al., 2003; the East Athabasca granulite terrane: Mahan and Williams, 2005; Flowers et al., 2006). Establishing comprehensive *P-T-t-D* (pressure-temperature-time-deformation) paths and quantifying metamorphic thermal and baric gradients are important prerequisites for exploiting these "field laboratories." The Upper Granite Gorge of the Grand Canyon is a 100% exposed cross section of six crustal blocks along an ~70-km-long transect. The cross section is interpreted to represent the mid-level of 30- to 40-km-thick continental crust at the culmination of the ca. 1.72–1.68 Ga Yavapai orogeny (Ilg et al., 1996), interpreted as a consequence of accretionary tectonism involving juvenile, island-arc terrane assembly of thin (15- to 25-km-thick) crustal fragments (Bowring and Karlstrom, 1990).

This contribution explores the significance of the tectonic blocks, their *P-T-t-D* evolution, and their high-strain zone boundaries with an emphasis on understanding the character, rheology, and exhumation of orogenic middle continental crust (Figs. 2 and 3). Previous work established the general structural and geochronologic framework for the region (Ilg et al., 1996; Hawkins et al., 1996; Ilg and Karlstrom, 2000). This paper focuses on a suite of samples with semipelitic to pelitic bulk compositions and utilizes detailed microstructural observations, high-resolution electron microprobe X-ray mapping, published petrogenetic grids, and quantitative absolute and relative thermobarometry to construct detailed *P-T-D* histories for each tectonic block. Data from each of the blocks, along with published geochronological data, demonstrate that a single, composite looping *P-T-t-D* path can be constructed for the entire Upper Granite Gorge. The results represent a new synthesis of the metamorphic evolution of Precambrian basement in the Grand Canyon. New techniques for reducing uncertainty in thermobarometry are applied to evaluate *P-T* differences between blocks with maximum precision (i.e., Worley and Powell, 2000). The present-day exposure represents a near-isobaric ~0.7 GPa level (~25 km paleodepths) of continental crust, exhumed to 0.3–0.4 GPa levels as a single, relatively coherent tectonic block by ca. 1.68 Ga.

GEOLOGIC BACKGROUND

The Upper Granite Gorge of the Grand Canyon is divided into six lithotectonic blocks, separated by NE-striking, steeply dipping, high-strain zones (Figs. 2 and 3) (Ilg et al., 1996; Hawkins et al., 1996). From southeast to northwest, these blocks have been named: Mineral Canyon, Clear Creek, Trinity Creek, Topaz Canyon, Tuna Creek, and Walthenberg Canyon (Figs. 2 and 3) (Hawkins, 1996). The tectonic features of the Upper Granite Gorge are attributed to an early event of thrusting (D_1), isoclinal folding, and penetrative NW-striking fabric development (S_1), followed by progressive subhorizontal contraction (D_2) and production of a NE-striking, steeply dipping foliation (S_2) associated with upright to overturned folds within blocks and subvertical high-strain zones between blocks (Ilg et al., 1996; Ilg and Karlstrom, 2000). Four granite pegmatite dike complexes occur within the six-block transect and locally intrude across some of the high-strain zone boundaries. From southeast to northwest, these are the Cottonwood, Cremation, Sapphire, and Garnet pegmatite complexes (Fig. 3) (Ilg et al., 1996). Locations in the Grand Canyon mentioned herein are designated by the number of river miles (RM) downstream of Lee's Ferry, Arizona.

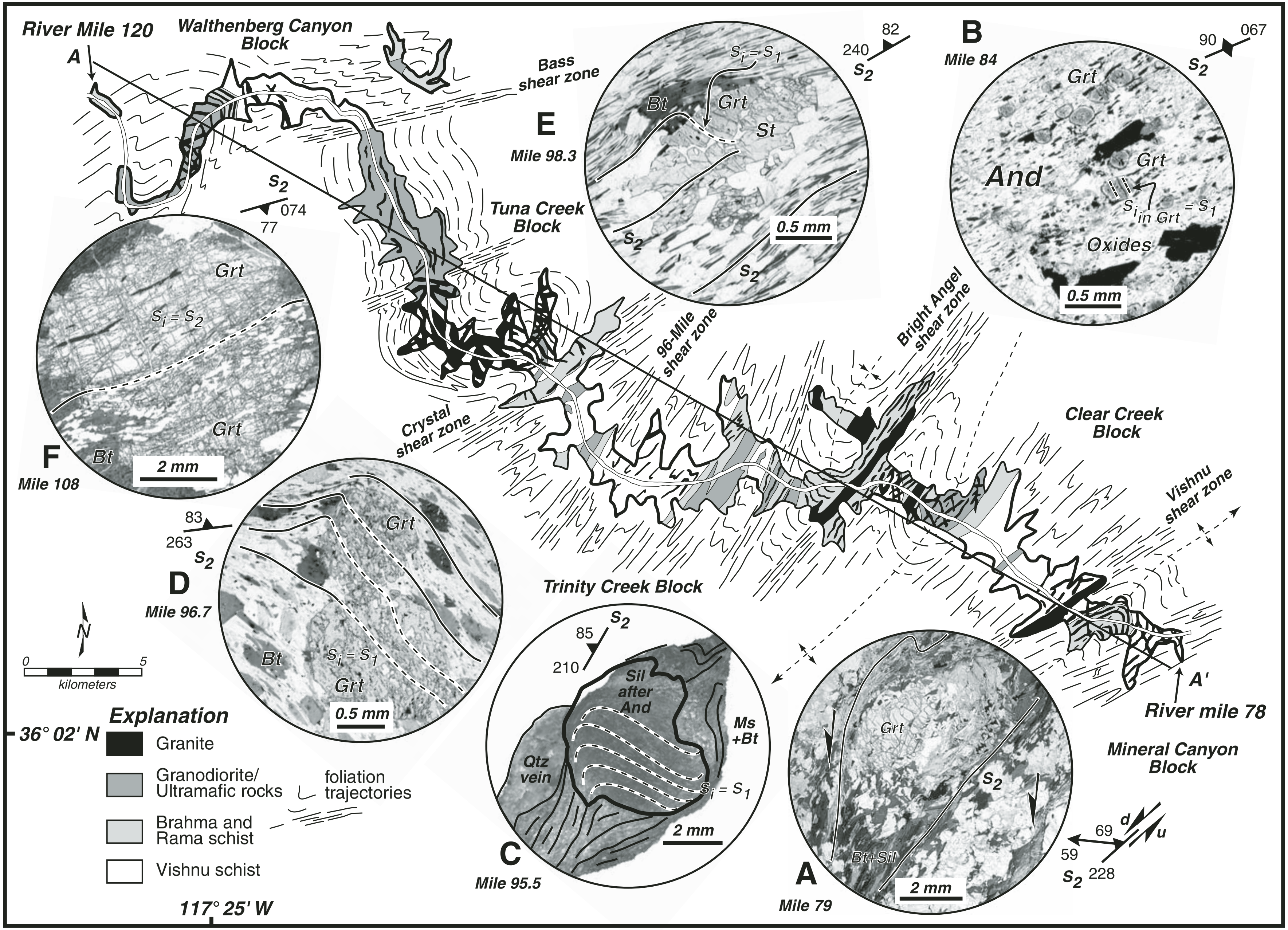

Figure 2. Simplified geologic map of Upper Granite Gorge with foliation trajectories (adapted from Ilg et al., 1996). Insets A through F illustrate key microstructural observations from field-oriented hand samples collected in each lithotectonic block discussed in the text. Inset A is a kinematic view of a thin section in plane-polarized light parallel to the mineral lineation and perpendicular to the foliation. Insets B and D–F are from map view thin sections in plane-polarized light oriented with respect to north on the map in the figure. Inset C is from a map view slab cut from a hand sample. Mineral abbreviations are after Kretz (1983).

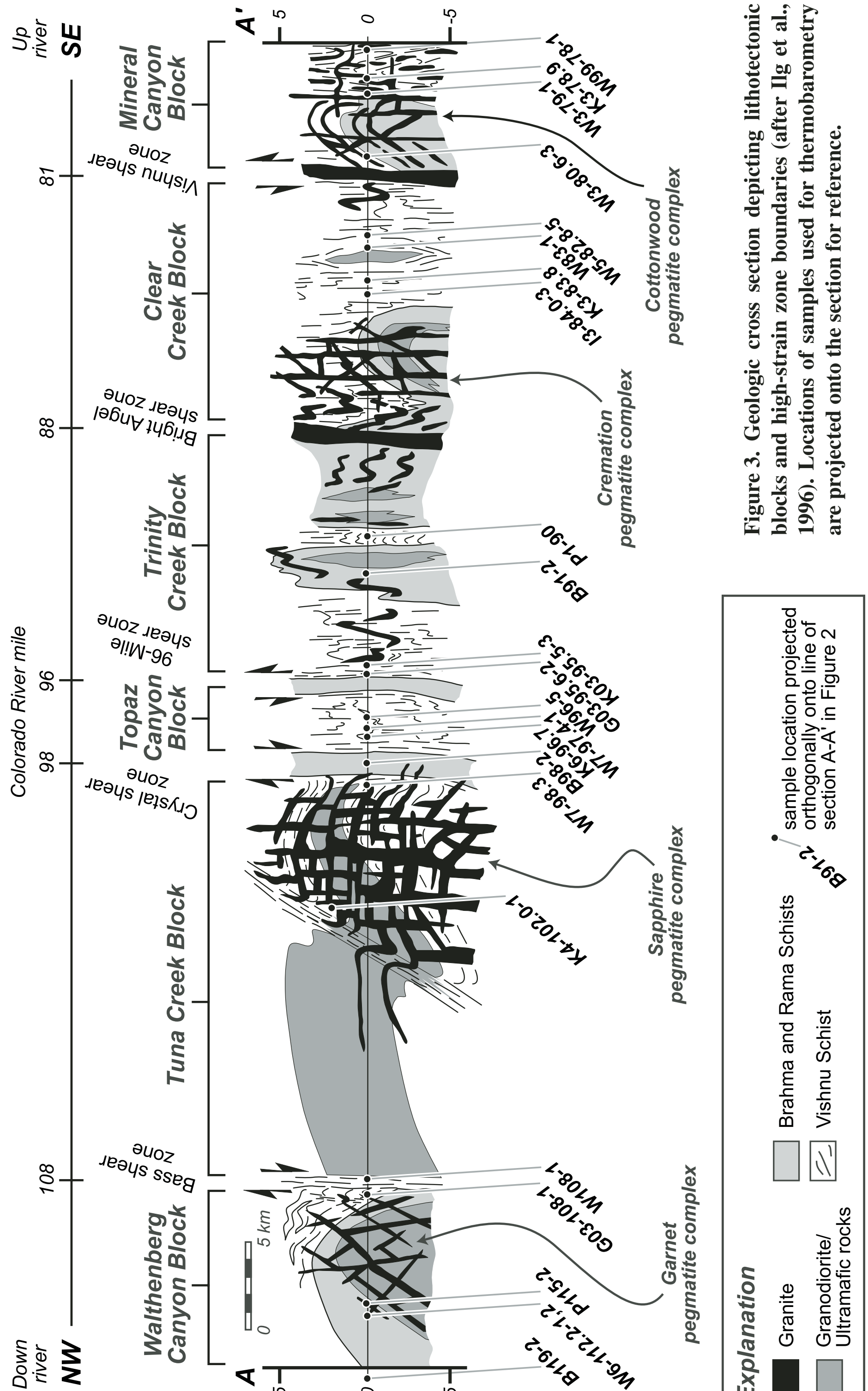

Figure 3. Geologic cross section depicting lithotectonic blocks and high-strain zone boundaries (after Ilg et al., 1996). Locations of samples used for thermobarometry are projected onto the section for reference.

Block-Bounding High-Strain Zones

Five high-strain zones characterized by intense subvertical, NE-striking, S_2-parallel foliation define boundaries between the six lithotectonic blocks. The Vishnu shear zone (RM 81: Fig. 3) marks the boundary between the Mineral Canyon and Clear Creek blocks. A penetrative NE-striking foliation in the host schist is defined by sigmoidal pods of sillimanite and muscovite after sillimanite. The muscovite is texturally late with respect to the peak assemblage but synkinematic with respect to deformation. New field work indicates sinistral sense of shear along a moderately SW-plunging lineation in these rocks adjacent to the eastern (up-river) margin of the tens-of-meters-thick Grapevine Camp pluton (1737 ± 1 Ma; Hawkins et al., 1996) (Fig. 2A). Sinistral, NW-side-down fabrics in the shear zone are cut by granitic dikes similar to ones dated by Hawkins et al. (1996) in the Mineral Canyon block at 1.685–1.68 Ga. The boundary between the Clear Creek and Trinity Creek blocks is defined by the Bright Angel shear zone (RM 88) (Figs. 2 and 3). The ~2-km-wide zone of penetrative migmatitic foliation experienced a component of dextral high-temperature movement inferred from microstructures and a macroscopic transposition of NW-striking S_1 fabrics (Ilg et al., 1996). The ~500-m-wide 96-Mile shear zone separates the Trinity Creek block from the Topaz Canyon block. The locally ultramylonitic zone records greenschist-grade, dextral (Karlstrom et al., 2003), and west-side-down movement (Dumond et al., 2004) (Fig. 3). The Topaz Canyon block is juxtaposed adjacent to the Tuna Creek block across the ~2-km-wide Crystal shear zone (RM 98). Apparent dextral, west-side-up movement is inferred from asymmetric folds and a map-scale deflection of S_1 foliation trajectories. Movement on the Crystal shear zone ceased by ca. 1.68 Ga based on the presence of crosscutting pegmatite dikes (Fig. 3) similar to those dated by Hawkins et al. (1996). Finally, the Bass shear zone (RM 108) separates the Tuna Creek block from the Walthenberg Canyon block. The ~0.5-km-wide shear zone records dextral, west-side-up motion in metasedimentary rocks adjacent to the northwestern margin of the ca. 1.717 Ga Ruby granodiorite pluton (Ilg et al., 1996; Hawkins et al., 1996).

Geochronologic Constraints on Timing of Magmatism, Deformation, and Metamorphism

Volcanogenic supracrustal rocks of the Upper Granite Gorge yield dates between 1750 ± 2 and 1741 ± 1 Ma (Hawkins et al., 1996). These rocks include the interlayered metavolcanic

Rama and Brahma schists and the metasedimentary (turbiditic) Vishnu schist. The age of D_1 is constrained by foliated arc-related plutons and crosscutting dikes to between 1730 ± 3 and 1698 ± 1 Ma (Hawkins et al., 1996). D_2 and the peak of metamorphism are constrained by dates on foliated granite plutons and crosscutting pegmatite dikes to between 1713 ± 2 and 1685 ± 1 Ma (Hawkins et al., 1996). Isotope dilution–thermal ionization mass spectrometry (ID-TIMS) U-Pb monazite and xenotime dates from leucosomes in migmatites constrain the timing of lower granulite-grade metamorphism in the Mineral Canyon block to between ca. 1702 and 1690 Ma (Fig. 3) (Hawkins and Bowring, 1999). Electron microprobe monazite ages from leucosomes near the Elves Chasm orthogneiss in the Walthenberg Canyon block (Fig. 3) support the age of peak metamorphism between ca. 1700 and 1680 Ma (Williams and Jercinovic, 2002). Undeformed granitic dikes dated between 1685 ± 1 and 1680 ± 1 Ma crosscut leucosomes in migmatites that define S_2 in the Mineral Canyon block (Fig. 3) (Hawkins et al., 1996). All geochronologic data are consistent with burial and peak metamorphism of middle continental crust during a protracted 20–30 m.y. period (ca. 1.71–1.68 Ga) of subhorizontal shortening and granitic plutonism.

METAMORPHIC PETROLOGY AND MICROSTRUCTURE

Utilizing this tectonic and geochronologic framework, we present petrologic and microstructural data pertaining to the tectonometamorphic evolution of the Upper Granite Gorge and place each block in the context of a *P-T-t-D* path. Of the over 700 samples available, 24 oriented samples of pelitic to semipelitic bulk composition that span the length of the transect were chosen for detailed analysis (Figs. 3 and 4; Table DR1[1]). High-resolution compositional X-ray maps of garnet and plagioclase were collected from all samples to assess major-element zoning and to locate the best regions from which to collect quantitative data (Fig. 4). Biotite compositions were collected both in the matrix and adjacent to garnet in order to evaluate the potential effects of retrograde net transfer reactions and to constrain the most appropriate choice for *P-T* calculations (i.e., Kohn and Spear, 2000). Representative compositions used for thermobarometry and analytical conditions are presented in Table DR1 (see footnote 1). All microprobe work was conducted using the Cameca SX-50 facility at the University of Massachusetts–Amherst. All pressures and temperatures (reported with 2σ uncertainties) were calculated using THERMOCALC 3.21 (average *P-T* approach of Powell and Holland, 1994; http://www.earthsci.unimelb.edu.au/tpg/thermocalc/) and the internally consistent thermodynamic data set of Holland and Powell (1998) with subsequent revisions. Activity-composition relationships were modeled at 0.6 GPa and 600 °C for all samples using the April 2000 version of AX (T. Holland, http://www.esc.cam.ac.uk/astaff/holland/ax.html). Possible thermal and baric gradients were evaluated using Δ*PT* "relative" thermobarometry software developed by Worley and Powell (2000). Mineral abbreviations are after Kretz (1983).

General Observations Regarding Medium- and High-Temperature Blocks

In general, field and petrographic observations, coupled with high-resolution X-ray maps, demonstrate that the blocks (or parts of blocks) can be divided into medium- and high-*T* varieties. All blocks display field and microstructural evidence for syn-D_2 growth of garnet in association with Bt + Pl + Qtz ± Ms (see also Ilg and Karlstrom, 2000). After summarizing general observations that pertain to medium- and high-*T* blocks along the transect, data unique to each tectonic block are presented in separate sections.

Medium-*T*, i.e., upper greenschist to lower amphibolite grade, regions along the transect include the up-river portion of the Clear Creek block (RM 81–85), the Topaz Canyon block (RM 96–98), and up-river portions of the Tuna Creek (RM 98–100) and Walthenberg Canyon blocks (RM 108–110). Typical peak mineral assemblages include Grt + Bt + Ms + Pl + Qtz ± St. Accessory phases include Mnz + Ap ± Xt ± Tur ± Ilm ± Zrn. Poikiloblastic chlorite locally occurs as a postkinematic phase overgrowing the S_2 foliation. With few exceptions, garnet porphyroblasts (up to 5 mm in diameter) contain uniformly NW-striking, straight to sigmoidal inclusion trails that occur at a high angle to the S_2 matrix foliation (Figs. 2D and 2E; Ilg and Karlstrom, 2000). At garnet rims, the internal fabric sweeps abruptly into the matrix orientation, which is consistent with synkinematic growth of garnet during D_2 (Fig. 2D). Locally, garnet crystals overgrow the steep S_2 matrix foliation (Fig. 2F). Samples least affected by retrograde resorption or diffusion exhibit increasing Mg-ratio from core to rim with decreasing X_{Mn} and X_{Ca}, which are typical of prograde growth zoning (see Spear, 1993; Kohn, 2003). Lath-shaped, normally zoned plagioclase (i.e., decreasing X_{Ca} from core to rim) is common throughout these regions, where it defines the predominant S_2 foliation along with biotite and muscovite (see zoning summary in Fig. 4). Muscovite and biotite crystals are generally unzoned, but in some cases, biotite compositions may vary with proximity to garnet (see Kohn and Spear, 2000). Biotite is variably altered to chlorite in most samples. Estimates of peak metamorphic conditions (summarized in the following sections and in Fig. 4) were calculated using garnet rim and plagioclase rim compositions with matrix biotite and muscovite.

High-*T*, i.e., upper amphibolite to lower granulite grade, conditions are preserved in the Mineral Canyon block (RM 77–81), the down-river portion of the Clear Creek block (RM 85–88), Trinity Creek block (RM 88–96), and the down-river portions of the Tuna Creek (RM 100–102) and Walthenberg Canyon blocks (RM 111–119). Typical peak mineral assemblages include Grt + Sil + Bt + Pl + Qtz ± Kfs ± Crd. Accessory phases include Mnz + Ap ± Xt ± Tur ± Ilm ± Zrn. Garnet porphyroblasts (up to 1 cm in diameter) occur throughout these sections of the Upper Granite Gorge and are commonly resorbed and inclusion-poor (Fig. 2A). Most crystals exhibit flat zoning profiles across garnet cores with abruptly decreasing Mg-ratio and increasing X_{Mn} near the rims, which are typical of retrograde zoning (e.g., Spear, 1993; Fig. 4). Anhedral plagioclase is reversely zoned in many samples (Fig. 4), and the penetrative foliation is commonly defined by biotite, laths of plagioclase, mats of fibrolite, prismatic sillimanite, and locally cordierite.

Except where noted, metamorphic conditions in high-*T* samples were calculated using core compositions for garnet and plagioclase with matrix biotite and/or muscovite for the following reasons: (1) Cores of garnet crystals are least affected by high-*T* diffusion of Fe and Mg or resorption of garnet during cooling and/or decompression (e.g., Kohn, 2003). These regions are typically the highest in Mg and lowest in Fe and Mn as observed in compositional X-ray maps. (2) Thermodynamic modeling in the system MnNCKFMASH for the assemblage Grt + Bt + Ms + Chl + Pl + Qtz demonstrates that in the absence of other Ca-bearing phases, growth of garnet necessarily leads to production of a more sodic plagioclase (Spear et al., 1991). The presence of distinct calcic rims on plagioclase, particularly near garnet, and the locally resorbed appearance of garnet in samples throughout the high-*T* blocks are consistent with breakdown of garnet and growth of anorthitic plagioclase during decompression (except where noted), and, hence, the sodic plagioclase

[1]GSA Data Repository item 2007007, silicate compositions, analytical methods, and color versions of Figures 5, 6, 8, 9, and 10, is available on the Web at http://www.geosociety.org/pubs/ft2007.htm. Requests may also be sent to editing@geosociety.org.

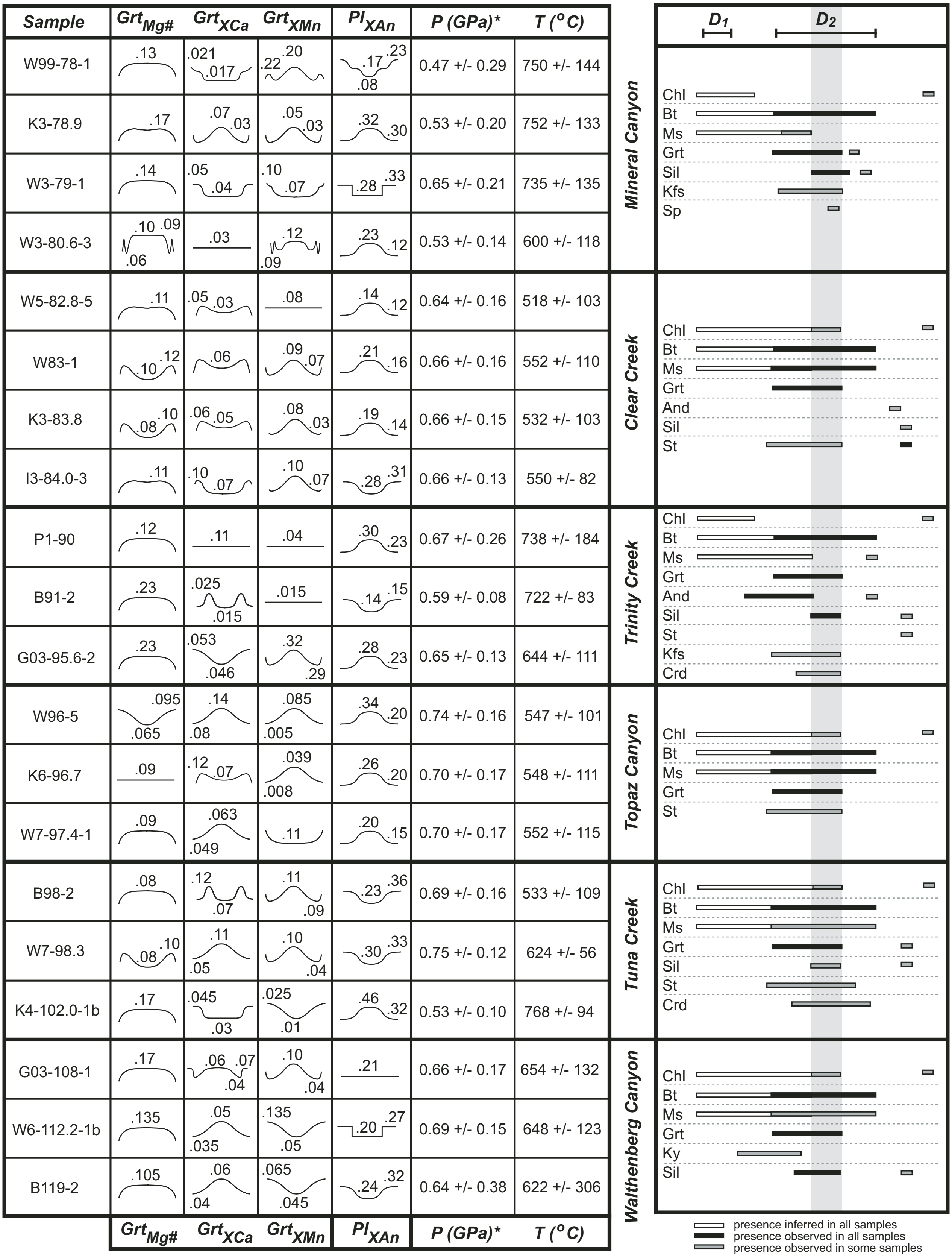

Figure 4. Summary of garnet (Grt) and plagioclase (Pl) zoning profiles, average pressure-temperature (*P-T*) estimates calculated from THERMOCALC 3.21 (Powell and Holland, 1994) with 2σ uncertainties, and observed/inferred mineral paragenesis for each lithotectonic block in the Upper Granite Gorge. Mineral abbreviations are after Kretz (1983).

cores best approximate the compositions that may have been in equilibrium with garnet near the metamorphic peak.

Mineral Canyon Block (RM 77–81)

The typical mineral assemblage in pelitic rocks of the Mineral Canyon block is Grt + Bt + Sil + Kfs + Pl + Qtz ± Spl, which suggests upper amphibolite– to granulite-facies conditions. Migmatitic textures are common with centimeter- to decimeter-scale lenses of leucosome distributed in paleosomal biotite- and sillimanite-rich schist (Ilg et al., 1996; Hawkins and Bowring, 1999).

Garnet porphyroblasts are commonly embayed and surrounded by plagioclase and/or K-feldspar, indicating significant retrograde garnet resorption (Figs. 5A and 5B; see Fig. DR1 for color version [see footnote 1]). Garnet compositional zoning varies depending on the size of the porphyroblasts. Although Mg-zoning is essentially flat for all garnet crystals, larger porphyroblasts (>5 mm) commonly preserve prograde zoning in Mn and Ca, whereas smaller porphyroblasts (<5 mm) display flat compositional profiles for all major elements. This is interpreted to be a consequence of compositional homogenization at high temperatures (Fig. 5B). Such zoning and the presence of resorbed textures are indicative of late Fe-Mg exchange and net transfer garnet-consuming reactions (Kohn and Spear, 2000; Kohn, 2003). In some samples, a marked increase in Ca across a sharp discontinuity occurs near the margins of garnet porphyroblasts. These rims are interpreted as a second generation of garnet (Grt 2 in Fig. 5A). They occur semicontinuously around embayed Grt 1 margins, including the margins of small isolated grains inferred to be relicts of the original Grt 1 porphyroblasts (e.g., Fig. 5A, upper right). These observations suggest that growth of Grt 2 occurred after significant resorption of Grt 1 had already occurred. The most abundant matrix plagioclase, commonly localized around garnet (Fig. 4; Pl 1 in Fig. 5A), is of intermediate anorthite content, and early sodic cores are locally present. Texturally latest and most calcic plagioclase (Pl 2 in Fig. 5A) is entirely restricted to the margins of garnet and specifically occurs where Grt 2 rims are narrow or absent. This is most consistent with a second stage of garnet resorption, consuming both Grt 1 and Grt 2.

Sillimanite occurs as dense mats of fibrolite distributed throughout the biotite-rich matrix. Clots of sillimanite and coarse biotite are typically concentrated around resorbed garnet porphyroblasts. In one sample, spinel is included in the outermost portion of garnet porphyroblasts. Quartz inclusions are abundant in the innermost portions and absent from the outer portions of the same garnet porphyroblasts, implying that spinel and quartz were not in equilibrium with one another. K-feldspar and plagioclase occur throughout the matrix in most samples. More calcic plagioclase also occurs as rims around relict K-feldspar cores in some samples. Muscovite is rare, although Hawkins and Bowring (1999) reported the local preservation of early muscovite largely replaced by sillimanite.

Phase Equilibria and P-T *Path*

Mineral assemblages and migmatitic textures indicate that rocks in the Mineral Canyon block underwent anatexis. Using textural observations and the petrogenetic grid developed by Spear et al. (1999) in the NKFMASH system, we infer a clockwise *P-T* path (Fig. 5C). Assuming insignificant free H_2O in the subsolidus system, melting is interpreted to have proceeded above invariant point 1 (IP1) via the Ms-dehydration melting reaction (Spear et al., 1999):

$$\text{Ms} \pm \text{Pl} + \text{Qtz} \rightarrow \text{Sil} + \text{Kfs} + \text{L}. \qquad (1)$$

The absence of Ms and the abundant association of Grt + Bt + leucosome are interpreted to represent completion of reaction 1 and the onset of melting via the Bt-dehydration melting reaction:

$$\text{Bt} + \text{Sil} \rightarrow \text{Grt 1} + \text{Kfs} + \text{L}. \qquad (2)$$

The presence of extensively resorbed garnet and clots of prismatic sillimanite and coarse biotite concentrated around garnet (Figs. 2A and 5A) may be attributed to reaction 2 operating in reverse (e.g., path 1 of Spear et al., 1999). Such a reaction crossed on the cooling and/or decompression path is likely responsible for the calcic plagioclase that is commonly localized around resorbed garnet margins. We infer one or more transient episodes of reheating following initial retrogression to explain the growth of Grt 2. These thermal spikes were then followed by continued cooling and decompression resulting in further retrogression of the high-*T* assemblage (Fig. 5C).

Peak metamorphic conditions were calculated from three samples using Grt + Bt + Sil + Pl + Qtz equilibria and yielded temperatures of 730–750 ± 144 °C and pressures of 0.47–0.65 ± 0.21 GPa (Fig. 4). In the sample illustrated in Figure 5, peak conditions were calculated at 735 ± 135 °C and 0.65 ± 0.21 GPa, whereas conditions calculated using Grt 2 and Pl 2 compositions are 637 ± 115 °C and 0.50 ± 0.18 GPa. The absence of late muscovite (outside of the Vishnu shear zone) implies that the retrograde path passed below IP1 (Fig. 5C), assuming that H_2O dissolved in the melt left the system upon crystallization (Spear et al., 1999).

Clear Creek Block (RM 81–88)

Peak mineral assemblages in the Clear Creek block indicate middle amphibolite–facies conditions from RM 81–85 grading to upper amphibolite–facies conditions from RM 85–88. The characteristic assemblage in the medium-*T* portion of the block includes Grt + St + Bt + Ms + Pl + Ilm + Qtz. The high-*T* portion of the block is characterized by Grt + Sil + Bt + Pl + Qtz (Ilg et al., 1996). Large (centimeter-scale) andalusite porphyroblasts, interpreted as postpeak and syn- to postkinematic (see following), occur in rocks near the mouth of Clear Creek Canyon (RM 84) (Figs. 2B and 6B). Dikes similar to the ones dated by Hawkins et al. (1996) at ca. 1.68 Ga at RM 80 are exposed in Clear Creek Canyon. These dikes are locally transposed into S_2 and boudinaged along L_2 (Ilg et al., 1996; this study).

Garnet porphyroblasts characteristically have an inclusion-rich core (Qtz + Ilm + Ap) and inclusion-poor rim (Fig. 6A; see Fig. DR2 for color version [see footnote 1]). The inclusion-poor garnet rims locally appear to have preferentially grown on the sides of garnet closest to staurolite (see following). Inclusion trails in garnet rims are parallel to the matrix fabric. Trails in garnet cores curve gradually toward the matrix/rim fabric (S_2) orientation (Fig. 6A). These observations are consistent with those of Ilg and Karlstrom (2000), who interpreted garnet to have grown during the development of S_2. The inclusion-poor overgrowths are characterized by higher grossular content (Figs. 4 and 6A).

Staurolite porphyroblasts (mm to cm scale) contain abundant inclusions and well-defined curvilinear inclusion trails similar to those in garnet (Fig. 6A). However, the trace of the innermost inclusion trail fabric commonly makes a smaller angle relative to the S_2 matrix foliation than the trace of the internal foliation in garnet cores in the same thin section (Fig. 6A). The margins of many staurolite porphyroblasts contain an inclusion trail fabric continuous with the matrix S_2 fabric (Fig. 6A). Partial resorption of staurolite is indicated by irregular margins and plagioclase-rich domains surrounding the porphyroblasts. Staurolite composition does not vary significantly across the grains. The microstructural observations suggest that staurolite growth began relatively later than garnet cores, having overgrown S_1 domains that were more transposed. Garnet rims grew during S_2 (i.e., concurrent with final transposition of S_1 domains) either after staurolite growth ceased or during breakdown of staurolite. The inferred paragenesis of garnet

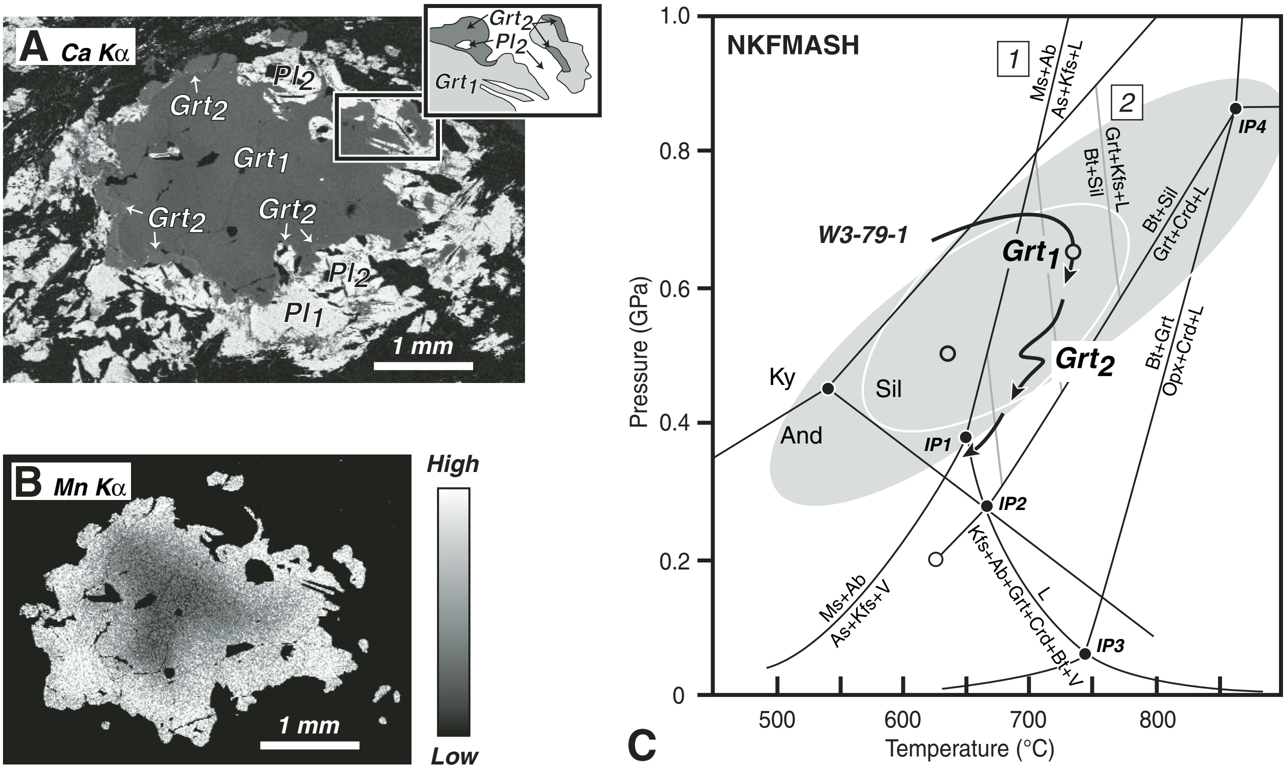

Figure 5. Summary of data and pressure-temperature (*P-T*) path for Mineral Canyon block. (A–B) High-resolution X-ray maps of garnet (Grt) and matrix. Lighter colors correspond to relatively greater concentrations of the element, and dark colors represent low concentrations in all X-ray maps. Calcium map in A illustrates two generations of garnet and plagioclase (Pl). Arrows point to sharp boundary between Grt 1 and Grt 2. (B) Map of retrograde Mn zoning in garnet. (C) Partial NKFMASH petrogenetic grid after Spear et al. (1999) with location of reactions 1 and 2 discussed in text. See Figure DR1 for color version of figure (see text footnote 1). Mineral abbreviations are after Kretz (1983). Note: IP1, IP2, and IP3 refer to invariant points in *P-T* space discussed by Spear et al. (1999).

growth, resorption, and regrowth in association with staurolite is supported by observations of relatively high-Y annuli in garnet coincident with the edge of inclusion-rich garnet cores. Resorption of early garnet left a zone in the matrix enriched in Y that was subsequently incorporated into garnet rims during renewed growth (i.e., Pyle and Spear, 1999).

Biotite occurs as a matrix phase aligned in S_2 and as millimeter-scale porphyroblasts that have curvilinear inclusion trail fabrics similar to garnet and staurolite. Muscovite and plagioclase are abundant matrix phases with compositions that do not vary significantly (Fig. 4).

Andalusite porphyroblasts up to 10 cm in diameter occur in outcrops in the vicinity of Clear Creek Canyon at RM 84. The porphyroblasts completely overgrow the dominant matrix S_2 fabric, suggesting post-D_2 growth (Fig. 2B). However, elongate andalusite porphyroblasts are locally boudinaged and pulled apart, with internal foliation that necks down into the matrix foliation, consistent with growth of some andalusite late during D_2 (Fig. 6B). The inclusion trail fabric is primarily defined by ilmenite with rare muscovite, biotite, and plagioclase. Garnet inclusions in the andalusite porphyroblasts contain inclusion-rich cores defining S_1 and high-Ca inclusion-poor rims, similar to matrix garnet (Fig. 2B). Fine-grained mats of randomly oriented fibrolite locally occur along grain boundaries between the host andalusite and its inclusions, as well as within late shear bands. The presence and orientation of these mats suggest a second period of sillimanite growth after andalusite.

Phase Equilibria and P-T *Path*

Mineral assemblages indicate that the upriver portion of the Clear Creek block experienced lower peak temperatures than the Mineral Canyon block. However, we infer a similar clockwise *P-T* path (Fig. 6C). Based on the textural evidence, growth of garnet cores was followed by staurolite and porphyroblastic biotite growth. This likely occurred via a reaction such as (i.e., the NKFMASH system modeled by Spear et al., 1999):

$$\text{Grt} + \text{Chl} \pm \text{Ms} \rightarrow \text{St} + \text{Bt}. \qquad (3)$$

This reaction implies that garnet growth ceased and was possibly consumed with increasing temperature. A period of garnet resorption is indicated by the occurrence of high-Y annuli outside the inclusion-poor garnet cores. Staurolite porphyroblasts show textural evidence for extensive resorption, while inclusion-poor garnet overgrowths imply a renewed period of garnet growth. Renewed garnet growth and staurolite consumption may have occurred via the reaction:

$$\text{St} + \text{Bt} \rightarrow \text{Grt} + \text{Ms} + H_2O. \qquad (4)$$

The significantly higher Ca concentrations in the garnet overgrowths (Fig. 6A) are interpreted to represent increasing pressure during this part of the path, based on contours of grossular isopleths in the MnNCKFMASH system for similar bulk compositions (Spear et al., 1991).

Thermobarometric calculations are remarkably consistent among four samples studied

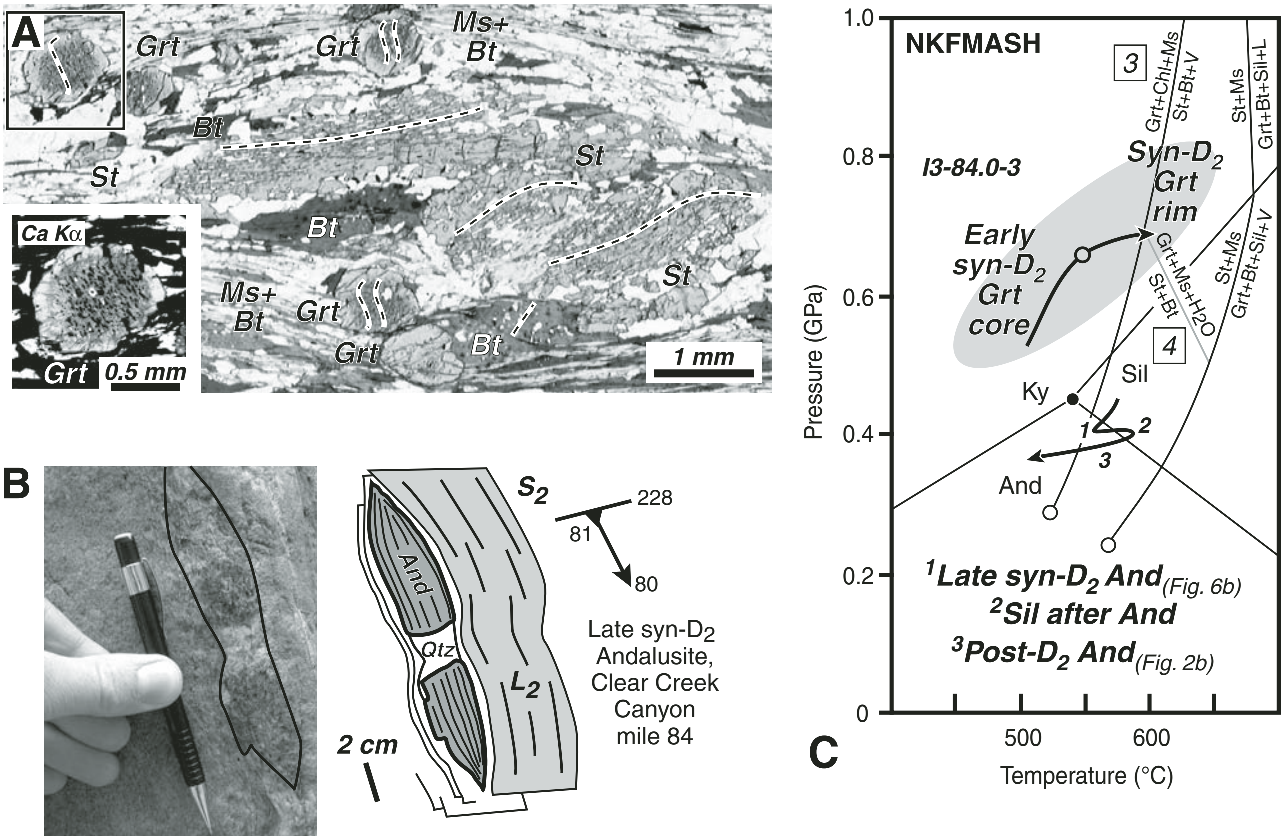

Figure 6. Summary of data and pressure-temperature (*P-T*) path for Clear Creek block. (A) Plane-polarized light photomicrograph from section cut perpendicular to foliation and parallel to lineation. Note trace of porphyroblast inclusion trails in staurolite (St) and garnet (Grt). Inset of Ca X-ray map depicts higher-Ca rim in Grt. (C) Partial NKFMASH petrogenetic grid after Spear et al. (1999) with location of reactions 3 and 4 discussed in text. See Figure DR2 for color version of figure (see text footnote 1). Mineral abbreviations are after Kretz (1983).

from RM 82–84 (Figs. 4 and 6C). Peak conditions were estimated using Grt + Bt + Ms + Pl + Qtz equilibria. Absolute temperatures range from 518 to 552 ± 110 °C. Calculated pressures range from 0.63 to 0.66 ± 0.16 GPa. The presence of late andalusite overgrowing garnet (Fig. 2A) indicates decompression to the andalusite stability field sometime after the passage of reaction 4. However, textural evidence for a second period of sillimanite growth after andalusite suggests a brief period of reheating at a pressure significantly lower than calculated pressures (Fig. 6C).

Trinity Creek Block (RM 88–96)

The Trinity Creek block is characterized by upper amphibolite– to lower granulite–grade assemblages (Grt + Sil + Pl + Bt + Qtz ± Crd ± Kfs) with local presence of sillimanite pseudomorphs after early andalusite, in addition to texturally late muscovite and staurolite. The area contains abundant leucocratic quartz segregations, pegmatite pods, and granitic dikes. Millimeter- to centimeter-scale elongate lenses of leucosome define and are locally wrapped by the main S_2 matrix foliation in some portions of the block. The lenses consist of randomly oriented quartz, K-feldspar, plagioclase, and biotite. Late muscovite porphyroblasts are commonly localized along the margins of the lenses. Poikiloblastic K-feldspar occurs locally in the leucosome and as a matrix phase.

Garnet porphyroblasts (<0.5 mm to 1.25 cm) are typically inclusion-free (Fig. 7A), but in some samples (e.g., sample B91–2), larger garnet porphyroblasts have texturally distinct cores that contain irregular inclusions of quartz. From sample to sample, garnet morphology ranges from deeply embayed to euhedral, demonstrating variable degrees of resorption. Mg-ratio is highest in the core and decreases dramatically at the margins. Mn zoning is generally flat for most garnet porphyroblasts, whereas some display a gradual decrease from core to rim. Grossular content is relatively low in the core and commonly increases toward the rim (Fig. 4).

In one cordierite-bearing sample (B91–2), garnet porphyroblasts contain prominent high-Ca annuli that occur just outside of inclusion-rich cores (Fig. 4). Cordierite occurs as porphyroblasts in textural equilibrium with garnet and matrix biotite (Fig. 7A). Muscovite is not present in this sample, in contrast to the more typical cordierite-absent samples throughout the block. Sillimanite occurs as inclusions in cordierite and as a fabric-defining matrix phase. Fine (<300 μm) euhedral staurolite and biotite grains occur along the margins of some cordierite porphyroblasts, and they are interpreted as a postkinematic retrograde assemblage.

Sillimanite occurs as elongate prismatic laths defining the dominant S_2 foliation in association with biotite in most samples. Fibrolitic mats of sillimanite occur as pseudomorphs of early millimeter-scale andalusite porphyroblasts in some samples (Fig. 7B). Sillimanite also occupies strain shadows adjacent to garnet and rare early muscovite porphyroblasts.

Field and petrographic observations are consistent with a single episode of early andalusite

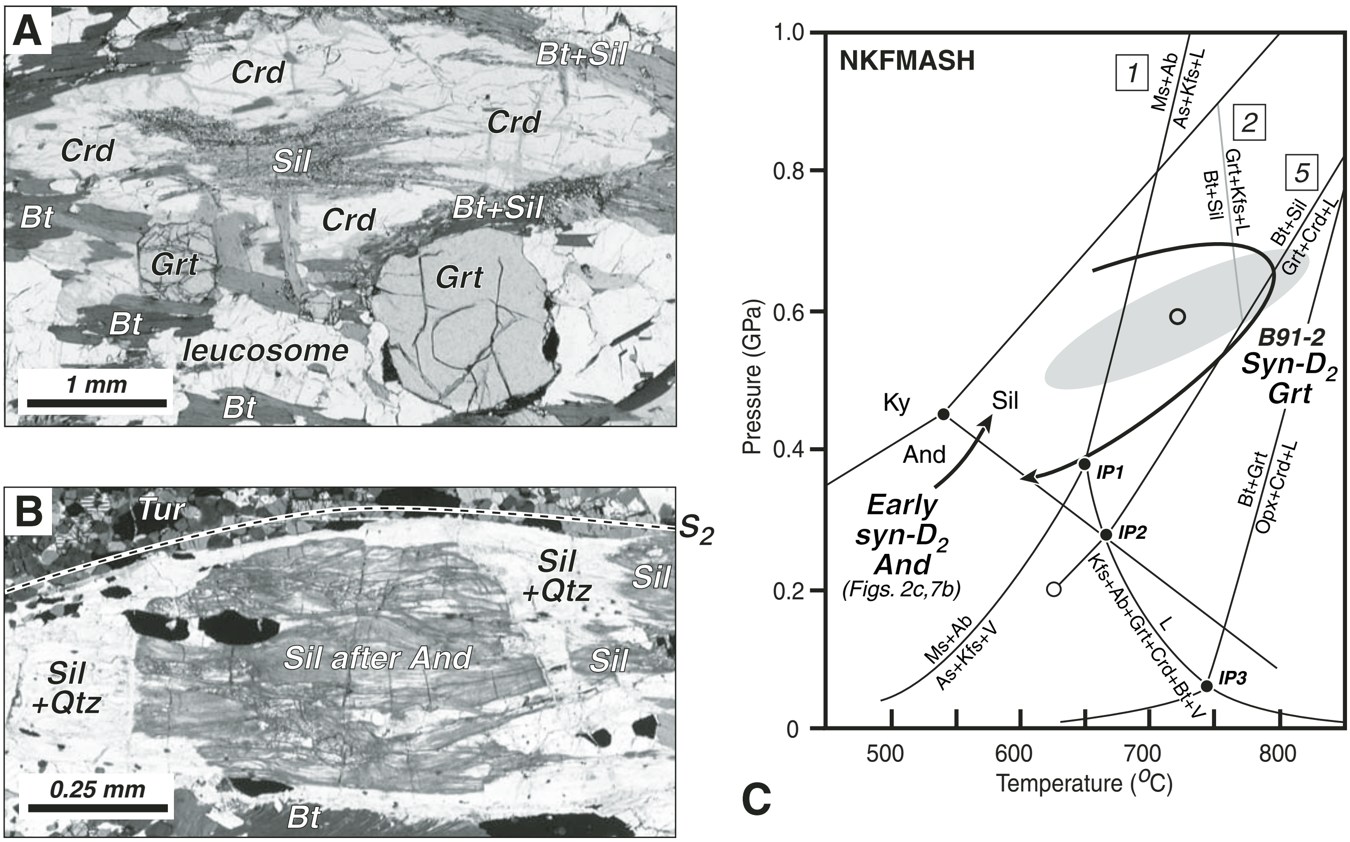

Figure 7. Summary of data and pressure-temperature (*P-T*) path for Trinity Creek block. (A–B) Plane-polarized light photomicrographs. Section in A is in plan view; section in B is oriented parallel to foliation and parallel to lineation. (C) Partial NKFMASH petrogenetic grid after Spear et al. (1999) with location of reactions 1, 2, and 5 discussed in text. Mineral abbreviations are after Kretz (1983).

growth in the Trinity Creek block. Pseudomorphs of andalusite replaced by sillimanite occur in 94-Mile Canyon (Fig. 7B). Beards of sillimanite and interstitial quartz occur in strain shadows of the pseudomorphs. South of the river at RM 95.5 in Travertine Canyon (sample K03–95.5–3 in Fig. 3), large (~5 cm in diameter) poikiloblastic andalusite porphyroblasts overgrow a NW-striking, steeply dipping inclusion trail (S_1). The internal fabric sweeps into the matrix foliation at the margins of the andalusite porphyroblasts, suggesting early synkinematic growth with respect to S_2 (Fig. 2C).

Phase Equilibria and P-T *Path*

Textural evidence for early andalusite indicates an early history of relatively low-pressure–high-temperature metamorphism (Fig. 7B). However, the relatively high-grade peak assemblage and leucosome textures in rocks from Trinity Creek block suggest that conditions of anatexis were attained. The absence of muscovite and abundance of sillimanite in the peak assemblage supports the passage of reaction 1 (in the NKFMASH system modeled by Spear et al., 1999) (Fig. 7C). High-Ca annuli in some samples, such as B91–2, may be explained by renewed garnet growth after passage of reaction 1 in the divariant field between reactions 1 and:

$$\text{Bt} + \text{Sil} + \text{Qtz} \rightarrow \text{Grt} + \text{Crd} \pm \text{Kfs} + \text{L}. \quad (5)$$

Because albite is consumed in reaction 1, renewed garnet growth must occur with higher grossular content in order to maintain equilibrium with new higher-Ca plagioclase (Spear et al., 1999) (Fig. 4). The local occurrence of Grt + Crd replacing sillimanite indicates that reaction 5 was reached in rocks of appropriate bulk composition (Fig. 7C).

Peak conditions were estimated using Grt + Crd + Sil + Pl + Bt + Qtz and yield 722 ± 83 °C and 0.59 ± 0.08 GPa (sample B91–2: Fig. 4). Unlike rocks in the Mineral Canyon block, most rocks in the Trinity Creek block contain abundant texturally late muscovite. This implies either: (1) the rocks cooled above IP1, so that crystallization of the remaining melt across reaction 1 provided the necessary H_2O for muscovite production (e.g., Spear et al., 1999), or (2) the system was not closed, and water was added at some later time. Textural evidence indicating syn- to late-D_2 muscovite growth suggests that muscovite was reintroduced shortly after peak metamorphism; this is most consistent with cooling above IP1. However, the difference in pressure between the Mineral Canyon and Trinity Creek blocks at this stage in the cooling history need not have been large (see path in Fig. 7C).

Topaz Canyon Block (RM 96–98)

The Topaz Canyon block experienced upper greenschist– to lower amphibolite–grade peak metamorphic conditions. No pegmatite dikes are exposed in the block, but two weakly foliated pre-D_2 granodiorite plutons are present: the 96-Mile pluton at RM 96.5 and the Crystal pluton at RM 97.5 (Hawkins, 1996). The predominant rock type is Grt + Bt + Ms + Pl + Qtz ± St ± Chl schist with a penetrative E- to NE-striking, steeply dipping foliation (S_2). Locally, the schist is associated with psammitic layering and graded bedding (S_0), which are interpreted as components of relict turbidite sequences (Ilg et al., 1996).

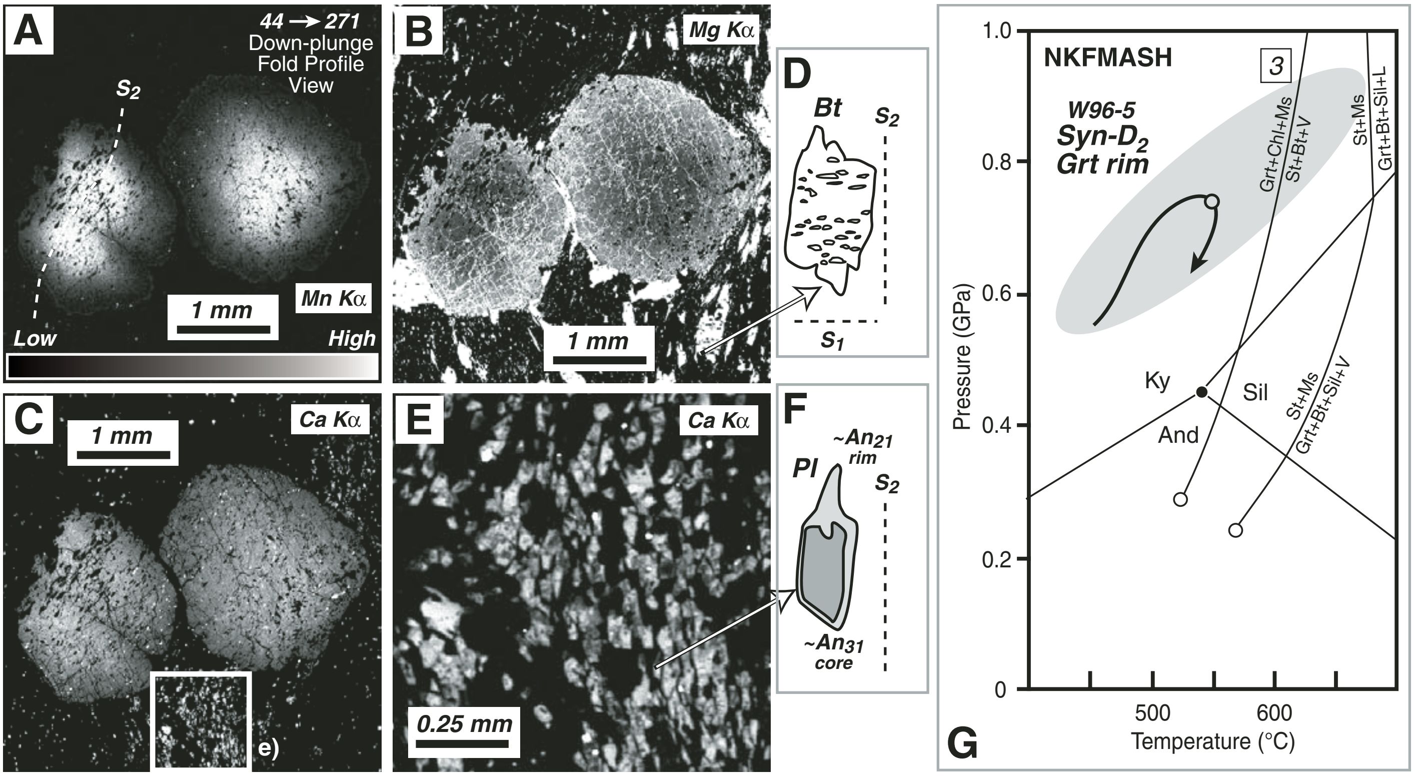

Figure 8. Summary of data and pressure-temperature (*P-T*) path for Topaz Canyon block. High-resolution X-ray maps for (A) Mn, (B) Mg, (C) Ca in garnet, and (E) Ca in matrix plagioclase. (D) Enlarged sketch of biotite porphyroblast from (B) highlighting preservation of subhorizontal inclusion trails. (F) Enlarged sketch of zoning in plagioclase in (E) highlighting alignment of sodic rims subparallel to S_2. Images are from a thin section cut perpendicular to the fold-axis. (G) Partial NKFMASH petrogenetic grid after Spear et al. (1999). See text for discussion and Fig. DR3 for color version of figure (see text footnote 1). Mineral abbreviations are after Kretz (1983).

Garnet porphyroblasts observed in oriented, map-view thin-sections contain uniformly NW-striking straight to sigmoidal inclusion trails that occur at a high-angle to the S_2 matrix foliation (Fig. 2D; Ilg and Karlstrom, 2000). At garnet rims, the internal fabric sweeps abruptly into the matrix fabric, which is consistent with synkinematic growth of garnet during D_2 (Fig. 2D). With few exceptions, most samples exhibit increasing Mg-ratio from core to rim, whereas X_{Mn} and X_{Ca} decrease from core to rim, typical of prograde zoning (Kohn, 2003; Figs. 4 and 8A–8C; see Fig. DR3 for color version [see footnote 1]).

Muscovite and biotite define a penetrative S_2 foliation. Locally, poikiloblastic biotite defines the S_2 cleavage and contains a subhorizontal inclusion trail, observed in fold-profile sections, which is inferred to represent the trace of S_1 foliation (Fig. 8D).

Plagioclase in the matrix is normally zoned with lath-shaped calcic cores and sodic overgrowths (Fig. 4). In sections cut perpendicular to the hinges of tight ENE-trending and moderately W-plunging F_2 folds, sodic rims characteristically occur as elongate overgrowths aligned with the S_2 cleavage (Figs. 8E–8F). The alignment is interpreted to reflect syn-S_2 growth of albitic plagioclase.

Phase Equilibria and P-T *Path*

Peak metamorphic conditions were calculated with the assemblage Grt + Bt + Ms + Pl + Qtz, utilizing garnet rims, matrix biotite and muscovite, and plagioclase rims (all inferred to represent syn-D_2 conditions based on our microstructural observations, e.g., Figs. 8A–8D). Calculated temperatures and pressures from four samples in the block range from 533 to 552 ± 115 °C and 0.69–0.74 ± 0.16 GPa (Figs. 4 and 8G). Some samples contain rare staurolite, implying that peak conditions locally approached ~550–600 °C (i.e., the staurolite-in isograd as defined by Spear and Cheney [1989] in the KFMASH system), within the uncertainty of calculated peak temperatures (Fig. 8g).

Samples from the Topaz Canyon block arguably contain the best-preserved examples of prograde syn-D_2 garnet in the entire transect, and thus provide the best approximation for peak pressure. Peak temperatures (~550 °C) were not high enough to reset primary titanite dated at 1714 ± 1 Ma in the 96-Mile pluton (Hawkins, 1996), in contrast to ca. 1.68 Ga titanite in the high-*T* Mineral Canyon block (Hawkins and Bowring, 1999) (closure temperature of ~550–660 °C; Cherniak, 1993). Together with the apparent lack of significant retrograde re-equilibration, these observations suggest that rocks from the Topaz Canyon block cooled relatively quickly after attaining peak pressure (e.g., *P-T* path for sample W96–5 in Fig. 8G).

Tuna Creek Block (RM 98–108)

The majority of the upper amphibolite–grade Tuna Creek block consists of the Ruby granodiorite pluton (RM 102–107.5) (1716.6 ± 0.5 Ma) and the Sapphire pegmatite complex (RM 99–102) (Hawkins et al., 1996). Two distinct assemblages occur in pelitic to semipelitic schists between the Crystal shear zone at RM 98 and the southeastern margin of the pluton at mile 102. Nearest to the Crystal shear zone, rocks consist of Grt + St + Bt + Ms + Pl + Qtz schist. Pelitic schists that host the Sapphire pegmatite complex at RM 102 contain Grt + Sil + Crd + Bt + Pl + Qtz.

Garnet porphyroblast textures and zoning in two-mica schists near the Crystal shear zone are similar to those observed in Topaz Canyon (e.g., sample W7–98.3: Figs. 2E, 4, and 9A; see Fig. DR4 for color version [see footnote 1]). Locally, however, garnet rims show marked increase in X_{Mn} at the rim (50–100 µm wide) (Fig. 4), which is typical of resorbed garnet zoning in the high-*T* blocks.

Plagioclase exhibits pronounced reverse zoning with lath-shaped sodic cores and distinct rim overgrowths of more anorthitic plagioclase (Fig. 9B). The schists contain abundant staurolite (texturally after garnet) with straight inclusion trails of quartz and plagioclase aligned with S_2 (Figs. 2E and 9A). Staurolite locally exhibits embayed margins and no compositional zoning (Table DR1, see footnote 1).

Cordierite-biotite schists further down-river (RM 102) contain subhedral to anhedral garnet, up to 5 mm in diameter, with abundant inclusions of quartz, apatite, biotite, oxides, monazite, and abundant sigmoidal mats of fibrolite (Figs. 9C–9D). Garnet crystals appear to be heavily resorbed, as indicated by relatively wide and irregularly shaped high-X_{Mn} rims that mimic the geometry of low-X_{Mg} rims (Figs. 4 and 9C). Most garnet crystals are homogeneous with respect to grossular content except for thin (up to 100 µm), high-Ca rims (Fig. 9E). These rims spatially coincide with a pronounced increase in Y. The high-Ca rims occur around most grains, including grains that texturally appear to have been part of once-larger garnet porphyroblasts, suggesting that they represent a second generation of garnet growth after initial garnet breakdown and resorption. These textures and zoning patterns are similar to those observed in the second generation of garnet in migmatitic samples of the Mineral Canyon block (RM 79, Fig. 5).

Plagioclase is normally zoned and defines the foliation along with abundant elongate

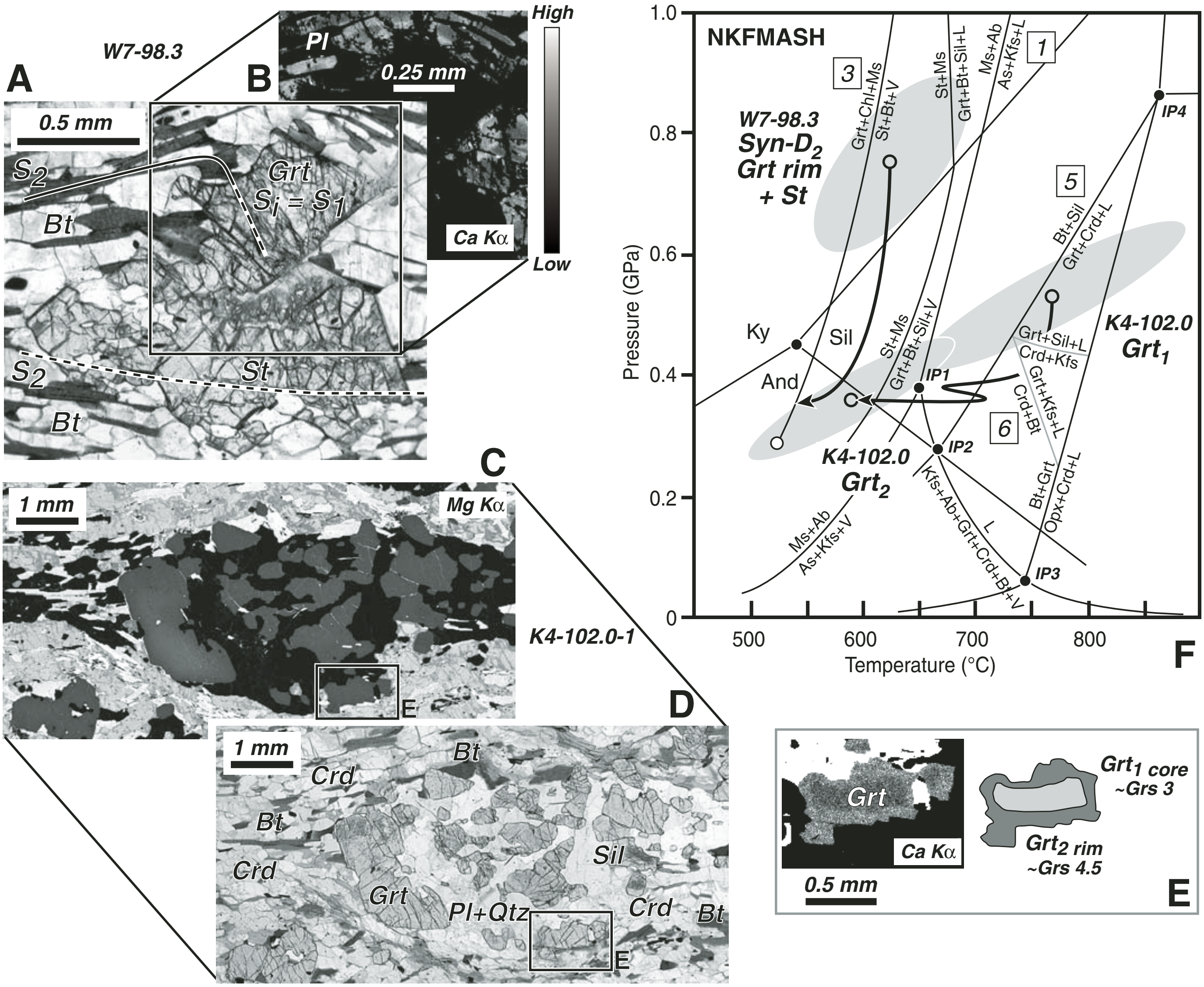

Figure 9. Summary of data and pressure-temperature (*P-T*) path for Tuna Creek block. (A, D) Plane-polarized light photomicrographs of sections cut perpendicular to foliation and parallel to lineation. (B) X-ray map of Ca in matrix plagioclase around garnet outlined in A. (C) Mg X-ray map keyed to part D. (E) Ca X-ray map of Grt in D with sketch depicting a low-Grs Grt core and slightly higher-Grs Grt rim separated by a sharp boundary. (F) Partial NKFMASH petrogenetic grid after Spear et al. (1999) with location of reactions 1, 3, 5, and 6 discussed in text. See Figure DR4 for color version of figure (see text footnote 1). Mineral abbreviations are after Kretz (1983).

cordierite crystals in schists that host the Sapphire pegmatite complex (Figs. 4 and 9C–9D; sample K4–102.0–1). Locally, cordierite makes up as much as 60% of the mode. The cores of many cordierite grains contain abundant inclusions of prismatic sillimanite and mats of fibrolite. Rims are typically altered to pinnite. Sillimanite also occurs in the matrix as prismatic laths and needles that define the foliation along with biotite. Samples near and within the pegmatite complex contain abundant leucosome (Grt + Pl + Qtz + Crd + Bt) textures mantled by Bt-rich selvages akin to paleosome, suggesting that some partial melting occurred. Garnet in leucosome is locally replaced by cordierite and biotite (Fig. 9C). K-feldspar and muscovite are absent from these samples.

Phase Equilibria and **P-T** *Path*

Samples W7–98.3 and K4–102.0–1 represent dissimilar bulk compositions, but are interpreted to preserve different parts of a similar *P-T* path for the Tuna Creek block as a whole (Fig. 9F). The presence of distinct calcic rims on plagioclase, particularly near garnet, and the locally resorbed appearance of garnet in W7–98.3 are consistent with breakdown of garnet and growth of anorthitic rims on plagioclase during decompression (Fig. 9A). Quantitative thermobarometry using Grt + Bt + Ms + Pl + Qtz equilibria and highest Mg-ratio rim compositions in garnet and core plagioclase compositions in sample W7–98.3 yield peak conditions of 624 ± 56 °C and 0.75 ± 0.12 GPa, which are consistent with the staurolite-in isograd (Spear and Cheney, 1989) (Figs. 4 and 9F).

Reaction textures in sample K4–102.0–1 can be interpreted using the same grid for anatectic pelites utilized for the Mineral Canyon and Trinity Creek blocks (i.e., Spear et al., 1999; Fig. 9F). The presence of abundant inclusions of biotite and mats of sillimanite in garnet hosted by matrix cordierite support the passage of reaction 5. In the presence of a partial melt, the following reaction may account for the observation of garnet replaced by cordierite and biotite in the leucosomes:

$$\text{Grt} + \text{Kfs} + \text{L} \rightarrow \text{Crd} + \text{Bt}. \qquad (6)$$

The lack of matrix K-feldspar implies that these rocks were heated at pressures above IP1, whereas the absence of retrograde muscovite implies the rocks cooled below IP1 ($P < 0.38$ GPa: Fig. 9F) (Spear et al., 1999). Alternatively, removal of melt results in a K-poor bulk composition; this explanation accounts for the K-feldspar–absent, restitic bulk composition of K4–102.0–1 (e.g., see also path 4 of Spear et al., 1999). *P-T* conditions calculated utilizing Grt + Sil + Crd + Bt + Pl + Qtz equilibria with garnet core, plagioclase rim, and matrix biotite compositions yield peak conditions of 0.53 ± 0.2 GPa and 769 ± 188 °C. As described earlier, garnet in K4–102.0–1 exhibits distinct high-Ca, high-Y rims attributed to a second phase of garnet growth (Fig. 9E). Pairing garnet and plagioclase rim compositions yields 590 ± 73 °C and 0.36 ± 0.08 GPa (Fig. 4).

Taken together, the two-mica schists and Crd + Bt schists provide evidence for a clockwise *P-T* path to ~0.7 GPa followed by decompression to ~0.3–0.4 GPa (Fig. 9F). Replacement of sillimanite and garnet by cordierite and the passage of reactions 5 and 6 imply decompression (i.e., Hollister, 1982; Spear et al., 1999). The second phase of garnet growth followed by resorption observed in K4–102.0–1 is attributed to reheating below IP1 (Figs. 9E and 9F).

Walthenberg Canyon Block (RM 108–119)

The Walthenberg Canyon block hosts the Elves Chasm orthogneiss (1840 ± 1 Ma) and the Garnet pegmatite complex (1697 ± 1 Ma) (Hawkins et al., 1996). An apparent metamorphic field gradient exists near the contact with the orthogneiss where Grt + Bt + Ms schists (e.g., sample W108–1, Fig. 2F, and sample G03–108–1, Fig. 4) grade into coarse migmatite (RM 115) with centimeter-scale garnet porphyroblasts mantled by tails of leucosome that contain K-feldspar, plagioclase, quartz, and biotite (sample P115–2 in Fig. 3; Williams and Jercinovic, 2002). Kyanite replaced by sillimanite occurs in an orthoamphibole-rich layer at RM 112 (Fig. 10A; see Fig. DR5 for color version [see footnote 1]), and is interpreted as an Al-rich weathering horizon (with ca. 1.75 Ga detrital zircon) that developed on Elves Chasm basement (Karlstrom et al., 2003). Metarhyolite layers east of and above the contact with Elves Chasm gneiss also contain kyanite replaced by sillimanite. Monazite dates from leucosomes at RM 115 range from ca. 1.7 to 1.68 Ga, suggesting that the field gradient is only "apparent" and reflects Yavapai-age peak metamorphism, rather than a contact aureole near the older Elves Chasm pluton (Williams and Jercinovic, 2002).

Garnet in Bt + Ms schists near the Bass shear zone (RM 108) and Bt + Ms + Ky/Sil schists (RM 112) that host the pegmatite complex contain inclusion trail relationships similar to those observed in the Topaz Canyon and Clear Creek blocks and are interpreted to reflect syn-S_2 growth of garnet (Figs. 2F and 10B). Cores of garnet locally display oscillatory zoning in grossular content with distinct high-Ca rims (G03–108–1, Fig. 4).

Plagioclase is zoned in all samples, with lath-shaped albitic cores that are aligned with S_2 and discontinuous anorthitic rims. X-ray maps of plagioclase demonstrate that the Ca-rich rims have sharp boundaries with the albitic cores (Fig. 10B).

Kyanite is observed as poikiloblastic, resorbed, and elongate blades in samples at mile 112 (Fig. 10A). Kyanite is locally mantled and replaced by muscovite, and elsewhere sillimanite occurs as pseudomorphs after kyanite (Fig. 10A). Throughout the Walthenberg Canyon block, in the vicinity of the Garnet pegmatite complex, sillimanite occurs as a foliation-defining matrix phase.

Phase Equilibria and **P-T** *Path*

The presence of early kyanite implies loading followed by breakdown to sillimanite (via muscovite). Textures and assemblages at RM 112 and RM 119 suggest that temperatures did not exceed those required for muscovite dehydration melting. In those areas, the common peak assemblage of Grt + Sil + Bt + Ms + Qtz is divariant in the NKFMASH grid of Spear et al. (1999). Thermobarometric estimates obtained from garnet and plagioclase core compositions in addition to matrix biotite yield conditions of 648 ± 123 °C and 0.69 ± 0.15 GPa (Figs. 4 and 10C). However, abundant leucosomes in Ms-absent samples at RM 115 demonstrate that partial-melting conditions were reached locally, pointing to the local passage of reaction 1 (e.g., sample P115–2, Fig. 3; Williams and Jercinovic, 2002). Figure 10C illustrates the preferred path for these rocks. The abundance of sharp, discontinuous anorthitic rims on plagioclase and texturally resorbed garnet in leucosome-absent samples (e.g., W6–112.2–1, Fig. 10B) are interpreted as consequences of decompression soon after peak conditions were reached (Fig. 10C).

DISCUSSION

Peak metamorphic conditions are commonly used to assess the magnitude of displacement across major structures as a step toward evaluating the tectonic significance of metamorphic field gradients (e.g., Todd and Engi, 1997; Fraser et al., 2000; Daniel et al., 2003; Tenczer and Stüwe, 2003). Next, we present a detailed comparison of thermobarometric results for the entire transect. We then describe how the *P-T* histories that we developed for each of the tectonic blocks (Figs. 5–10) can be used to constrain a composite looping *P-T-t-D* path for the entire Upper Granite Gorge. The results provide important constraints for: (1) the block-type architecture of continental crust in the

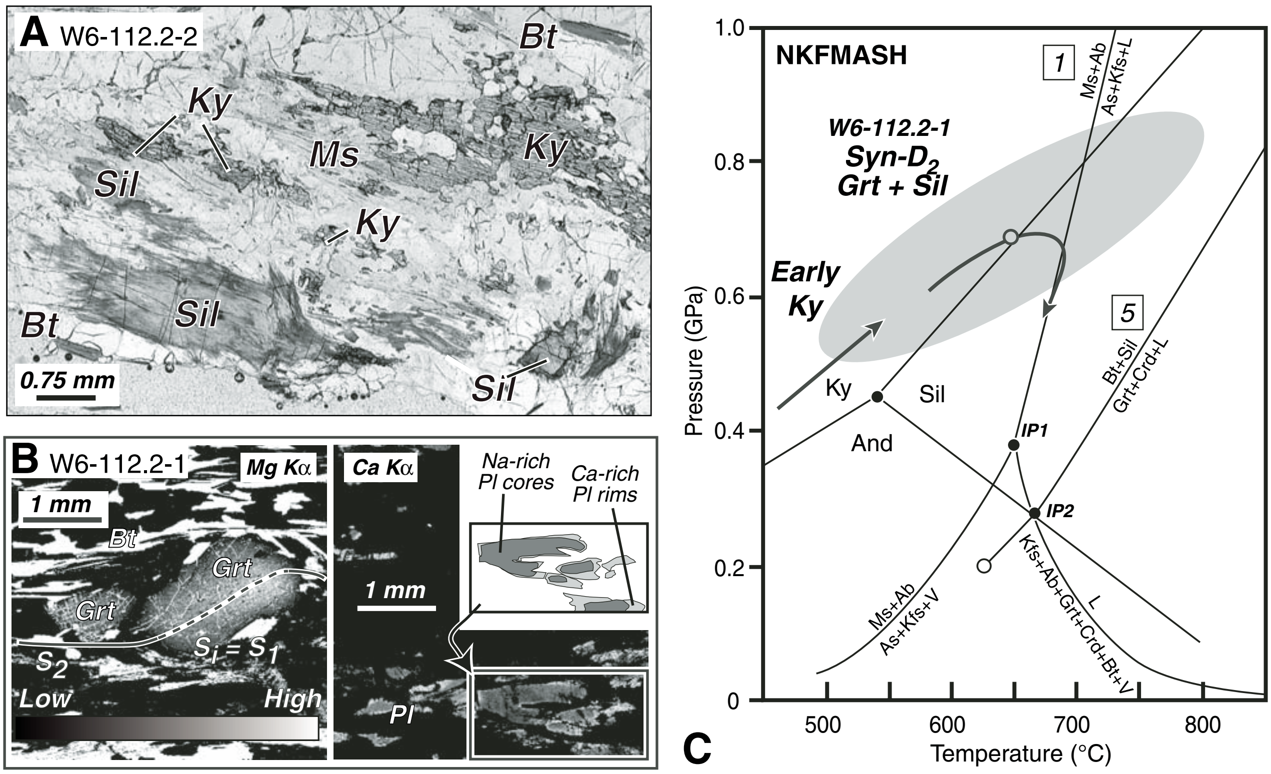

Figure 10. Summary of data and pressure-temperature (*P-T*) path for Walthenberg Canyon block. (A) Plane-polarized light photomicrograph illustrating reaction texture of Ky → Ms → Sil. (B) High-resolution X-ray maps of Mg in garnet and Ca in matrix plagioclase. Note trace of inclusion trail in garnet and distinct Ca-rich overgrowths on plagioclase. (C) Portion of NKFMASH petrogenetic grid after Spear et al. (1999). See text for discussion and Figure DR5 for color version of figure (see text footnote 1). Mineral abbreviations are after Kretz (1983).

Paleoproterozoic, (2) the rheology of middle continental crust during orogenesis, and (3) the denudation of orogens and preservation of isobaric levels of continental crust.

Comparison and Evaluation of Thermobarometric Data

Field and petrographic observations suggest that peak temperatures varied significantly along the transect and that thermal transitions coincided, in some cases, with block boundaries. Elsewhere, the transitions more closely coincided with dense pegmatite dike complexes (see also Ilg et al., 1996). However, traditional estimates of peak conditions and uncertainties do not have sufficient resolution for evaluating the tectonic significance of block boundaries in the Upper Granite Gorge. With few exceptions, differences in *absolute* temperature and pressure are indistinguishable at the 2σ level of uncertainty (Figs. 11A and 11C). A technique for comparing calculated *P-T* conditions from samples with the same mineral assemblage or subassemblage has been developed recently (the Δ*PT* approach: Worley and Powell, 2000). Utilizing the same mineral assemblage, activity-composition models, and internally consistent thermodynamic data set, much of the systematic error in thermobarometry can be eliminated. One sample is chosen as a "baseline sample" against which all other samples are compared. The approach yields more precise estimates of *differences* in pressure and temperature, providing a means to quantitatively evaluate thermal and baric gradients inferred from mineral assemblages and absolute thermobarometry (Hodges and McKenna, 1987).

The bulk of the samples studied from the Upper Granite Gorge contains one of the following peak mineral assemblages or subassemblages: Grt + Sil + Bt + Pl + Qtz or Grt + Bt + Ms + Pl + Qtz. Sample W6–112.2–1 was chosen as the baseline sample because all phases in both assemblages are inferred to have been in equilibrium at the peak of metamorphism; both subassemblages also yield nearly the same calculated *P-T* conditions. Water is excluded, and only fluid-conserved equilibria are used for these calculations, which involve the following mineral end members as specified in THERMOCALC: Ms, Cel, Phl, Ann, East, Py, Alm, Gr, An, Sil, and Q (see also Worley and Powell, 2000). Results are illustrated at the 2σ level of uncertainty (Figs. 11B and 11D).

Relative Thermometry (Δ*T*)

The Δ*T* results show a significant improvement in the resolution of temperature differences from block to block (Fig. 11B). Peak temperatures of high-grade samples from the Mineral Canyon, Trinity Creek, and Tuna Creek blocks all statistically exceed the baseline sample (W6–112.2–1 = 639 °C) at the 95% confidence level. Most of the remaining samples are significantly below the baseline. Many of the high-*T* samples are spatially coincident with the Cottonwood (RM 79–81), Cremation (RM 86–90), and Sapphire pegmatite complexes (RM 98–102). Samples at RM 90–91 in the Trinity Creek block are also spatially associated with centimeter-scale leucosomes, granitic veins, and pegmatite pods that are near the down-river extent of the Cremation pegmatite complex. Thus, the results support field observations that entire high-*T* blocks and portions of other blocks correspond to regions with a higher density of granitic pegmatite pods and dike complexes, as suggested by Ilg et al. (1996), e.g., the high-*T* Trinity Creek

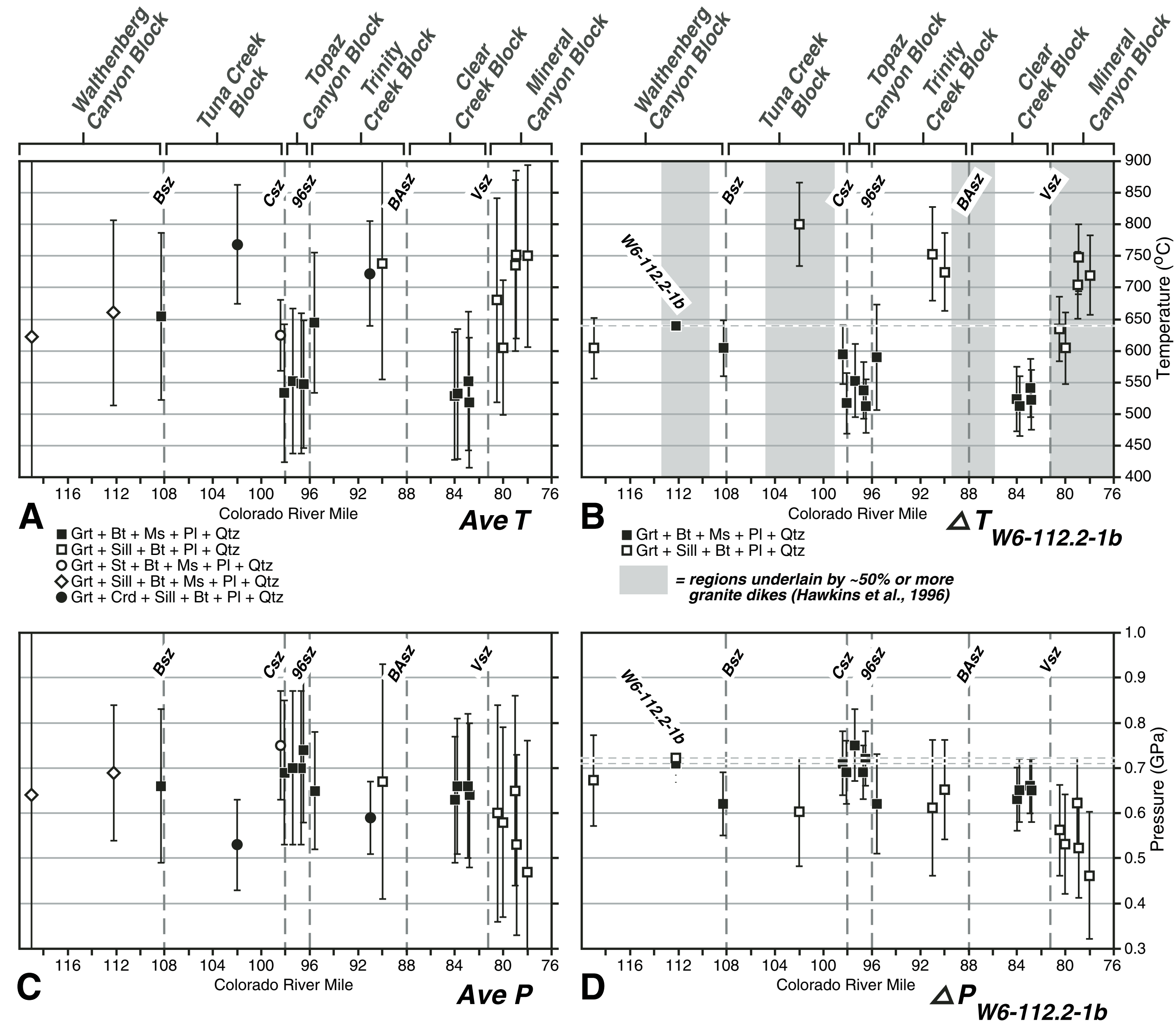

Figure 11. Comparison of pressure-temperature (*P-T*) results across the Upper Granite Gorge transect. (A) Average *T* for all samples as reported in Figure 4 with full mineral assemblage. (B) Δ*T* results for samples containing the appropriate subassemblage discussed in the text. Baseline sample at mile 112 yields the same result for both mineral subassemblages in Δ*T* plot at right (i.e., 638 °C for Grt + Bt + Ms + Pl + Qtz versus 639 °C for Grt + Sil + Bt + Pl + Qtz). (C) Average *P* for all samples as reported in Figure 4 with full mineral assemblage. (D) Δ*P* results across the Upper Granite Gorge transect. Bsz—Bass shear zone; Csz—Crystal shear zone; 96sz—96-Mile shear zone; BAsz—Bright Angel shear zone; Vsz—Vishnu shear zone.

block versus the medium-*T* Topaz Canyon block (compare Fig. 11B with Fig. 3).

Relative Barometry (Δ*P*)

Relative pressures for the Upper Granite Gorge are illustrated in Figure 11D. Even with the increase in precision, the pressures are essentially indistinguishable at the 2σ level throughout the entire transect. Most samples plot on or within ~0.05–0.1 GPa of the baseline sample (W6–112.2–1 = 0.71 GPa). Slightly lower pressures are recorded in the highest temperature samples. This is interpreted to be a consequence of either or both of the following: (1) re-equilibration and/or growth of new garnet at postpeak conditions, as documented in samples near RM 77–80, 90–95.6, 102, and 108; and/or (2) the clockwise *P-T* path, whereby the equilibrium pressure recorded at maximum temperature in a sample is commonly lower than the maximum pressure achieved (Spear et al., 1984). Based on these results, we infer that samples from the high-*T* blocks experienced similar pressures as samples in the medium-*T* blocks, which implies that the entire Upper Granite Gorge transect represents a near-isobaric, i.e., subhorizontal (0.7–0.65 GPa

≈25 km paleodepth), level of continental crust. The lack of distinguishable pressure variation precludes any amount of significant syn- to postpeak vertical displacement along the high-strain zones. Mesoproterozoic to Phanerozoic tectonic events (e.g., reactivation of the 96-Mile shear zone [Dumond et al., 2004], Laramide monoclines, and/or differential erosion) were insufficient to juxtapose different crustal levels, i.e., relative vertical displacements were on the order of ~3 km or less (0.1 GPa ≈3–4 km).

Implications of Δ*PT* Results

Apparent gradients and discontinuities revealed by the Δ*T* results can most likely be attributed to one or both of two possibilities: (1) postpeak strike-slip displacement along block-bounding shear zones juxtaposing samples in hotter tectonic blocks adjacent to samples in colder tectonic blocks, or (2) proximity of a sample to locally elevated thermal regimes caused by intrusion of 1.698–1.680 Ga granite dike complexes. As mentioned already, the Δ*P* results preclude significant dip-slip movement (>3–4 km) on the block-bounding shear zones.

Abrupt thermal discontinuities exist across the Vishnu shear zone (as noted by Ilg et al., 1996), which suggest a relatively significant amount of postpeak displacement. The shear zone coincides with an abrupt decrease in pegmatite density from SE to NW (Ilg et al., 1996), traversing down-river out of the Cottonwood pegmatite complex (Fig. 3). Field observations demonstrating sinistral sense of shear along a moderately SW-plunging lineation (Fig. 2A) and postpeak synkinematic muscovite are most consistent with focused fluid influx in the shear zone concurrent with postpeak, oblique-slip displacement. Thus, spatially heterogeneous advective heat from the Cottonwood pegmatite complex and displacement across the shear zone may have both contributed to development of a thermal discontinuity across the Vishnu shear zone. A second thermal discontinuity occurs across the 96-Mile shear zone (Fig. 11B). Sample G03–95.6–2 on the up-river side of the shear zone in the Trinity Creek block overlaps the baseline sample (Fig. 11B), in contrast to the three samples studied from the down-river side of the shear zone in the Topaz Canyon block, which all record lower temperatures. This is consistent with postpeak displacement on the 96-Mile shear zone inferred by Ilg et al. (1996) and confirmed by Dumond et al. (2004).

Thermal gradients across other block boundaries are coincident with the location of dense pegmatite complexes and boudinaged granitic pods. Pegmatite complexes intrude into and/or across the Bright Angel and Crystal shear zones (compare Figs. 3 and 11B). Amphibolite-grade assemblages occur on either side of the Bright Angel shear zone, and sillimanite-bearing rocks occur in the Clear Creek block between RM 86 and 88. Collectively, the Δ*PT* results are most consistent with flux of a laterally varying source of heat in a subhorizontal section of middle continental crust that experienced minor vertical offset and local transcurrent displacement along block-bounding high-strain zones. The important role of heat advection by ascending magma has been emphasized for several metamorphic terranes, e.g., the Central Maine Belt, USA (Johnson et al., 2003) and the Arunta Inlier of central Australia (Collins and Vernon, 1991). The absence of significant differences in pressure coupled with large differences in temperature along the Upper Granite Gorge transect result in a stark contrast to other orogens that are characterized by a relatively large variation in pressure and little variation in peak temperature (e.g., the High Himalayan metamorphic sequence, Fraser et al., 2000; the Lepontine–central Alps, Todd and Engi, 1997; the Koralpe region–eastern Alps, Tenczer and Stüwe, 2003).

Composite Looping *P-T-t-D* Path for the Entire Upper Granite Gorge Transect

Rocks from the Upper Granite Gorge have been used to place constraints on the regional *P-T-D* history (Fig. 12A). Although no single tectonic block preserves a complete record of its *P-T-D* history, there are a number of important similarities among the blocks. Each block shows evidence for a similar clockwise *P-T* path with at least some decompression after the metamorphic peak. We suggest that a single looping style of *P-T* path can explain the observations from all tectonic blocks (Fig. 12B). The path involves an early stage of tectonic loading with pressure increasing to ~0.7 GPa followed by decompression to ~0.3–0.4 GPa and a period of near-isobaric cooling. The looping geometry of the path is characteristic of much of the Paleoproterozoic basement of the southwestern United States (Williams and Karlstrom, 1996). Pressures during the early stages of metamorphism varied from region to region, but essentially all regions resided at 10–15 km depths (i.e., ~0.3–0.4 GPa) from ca. 1.65 to 1.4 Ga (Williams and Karlstrom, 1996).

Following deposition of volcanogenic and turbiditic supracrustal rocks between ca. 1750 and 1740 Ma (#1 in Fig. 12B), rocks were transported to middle crustal depths during two overlapping periods of deformation: (1) penetrative NW-striking fabric development, thrusting, and isoclinal folding (D_1) between 1730 and 1700 Ma (inferred here to represent the tectonic thickening of originally thin, juvenile crust, i.e., Bowring and Karlstrom, 1990), and (2) protracted subhorizontal shortening accompanied by steep NE-striking fabric development (D_2) between 1713 and 1685 Ma (Ilg et al., 1996). The presence of early syn-D_2 andalusite (Fig. 2C) indicates that the transition from NW- to NE-striking fabrics occurred relatively early and at relatively low pressures in the overall tectonometamorphic history of the transect (#2 and #3 in Fig. 12B).

The composite *P-T-t-D* path illustrates: (1) the similarities and differences between each block's history, (2) the unique combination of data that each block provides about the Upper Granite Gorge in general, and (3) the series of thermal spikes attributed to flux of magma through dense pegmatite dike complexes between 1.7 and 1.68 Ga. The prograde part of the path was different for various parts of the transect. For example, early kyanite was replaced by sillimanite in the Walthenberg Canyon block (Fig. 10A), but sillimanite replaced andalusite in the Trinity Creek block (Fig. 7B). The approach to peak conditions was controlled by both the degree of heating and the rate of loading along the prograde part of the path (e.g., the two example dashed paths at the origin of the *P-T-t-D* diagram in Fig. 12B). Differences between initial *P-T* path trajectories from block to block can also be attributed to the degree and style of thrust-imbrication during D_1, as described by Ilg et al. (1996) and Duebendorfer et al. (2001).

The upper pressure limit on the prograde portion of the clockwise *P-T-t-D* path is best constrained by near-peak pressure estimates of ~0.7 GPa from prograde syn-D_2 garnet in the Clear Creek and Topaz Canyon blocks (Figs. 6 and 8). The timing of peak metamorphic conditions is best constrained from leucosomes dated in migmatitic rocks from opposite ends of the transect: 1702–1690 Ma based on isotope dilution–thermal ionization mass spectrometry (ID-TIMS) analysis of monazite and xenotime in the Mineral Canyon block (Hawkins and Bowring, 1999) and ca. 1700–1680 Ma from electron microprobe dating of monazite in the Walthenberg Canyon block (Williams and Jercinovic, 2002) (#4 in Fig. 12B). These conditions were followed by a period of decompression as inferred by garnet + sillimanite breakdown to cordierite in the Tuna Creek block and evidence throughout the Upper Granite Gorge for breakdown of garnet to plagioclase. Decompression to andalusite stability is best constrained in the Clear Creek block, where late syn-D_2 to post-D_2 andalusite occurs (Figs. 2B and 6B). Combined with the presence of early-D_2 andalusite in the Trinity Creek block, the observations imply that relatively rapid burial from andalusite stability to peak pressure and decompression to andalusite stability occurred *entirely* during D_2. The

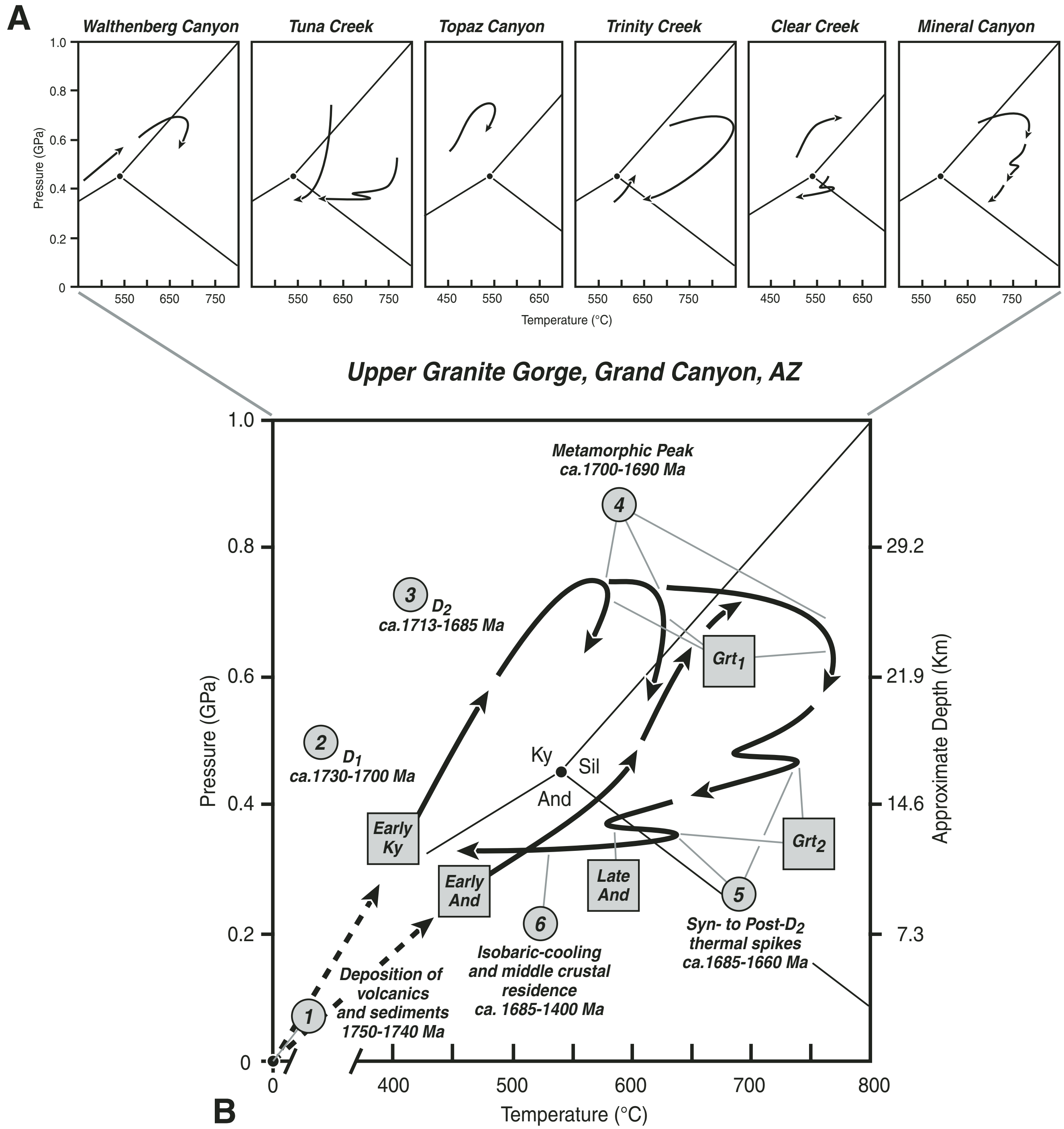

Figure 12. (A) Summary of path geometries interpreted for each lithotectonic block. (B) Composite *P-T-t-D* (pressure-temperature-time-deformation) path for entire Upper Granite Gorge, Grand Canyon, Arizona, USA. See text for discussion.

timing of decompression is best constrained by ca. 1.685–1.68 Ga undeformed dikes that cut D_2 fabrics in the Mineral Canyon block.

The stark differences in metamorphic grade correspond spatially with proximity to dense pegmatite dike swarms and/or boudinaged granitic pods (Fig. 11B; Ilg et al., 1996); this observation suggests that preserved thermal variations along the transect are due, in part, to variable degrees of advective heating. Thermal "spikes" along the retrograde path are interpreted to be the cause of the second generation of garnet documented in the Mineral Canyon and Tuna Creek blocks (#5 in Fig. 12B), i.e., flux of magma during dike emplacement provided the heat necessary to drive garnet-producing divariant reactions during decompression to 0.3–0.4 GPa (see paths in Figs. 5C and 9F). Late fibrolite and prismatic sillimanite in the Tuna Creek block plus sillimanite after post-D_2 andalusite in the Clear Creek block are consistent with this interpretation. The thermal spikes were most likely transient and varied both spatially and temporally with the distribution and timing of pegmatite dike intrusions. We suggest that these "spikes" along the *P-T-t-D* path may be a common phenomenon in orogenic belts with abundant syn- to postmetamorphic intrusive rocks (e.g., Williams and Karlstrom, 1996; Whitney and Dilek, 1998).

CONCLUSIONS

Several important insights emerge from the data. (1) The entire Upper Granite Gorge transect followed a looping *P-T-t-D* path in which all blocks reached a pressure of ~0.7 GPa by 1.70–1.69 Ga. All six tectonic blocks form a single, relatively coherent terrane of ~25-km-deep Paleoproterozoic middle continental crust. (2) Peak temperatures record lateral variations in temperature of greater than 250 °C (~520–770 °C) and were influenced by local advection of heat through pegmatite dike complexes along with local transcurrent movement on block-bounding shear zones. (3) The entire subhorizontal section of continental crust was decompressed to ~0.3–0.4 GPa (exhumed to ~12 km depths) between ca. 1.7 and 1.68 Ga. (4) Microstructural data indicate that D_2 shortening took place throughout the entire ~15–20 m.y. interval of peak metamorphism and subsequent decompression. These conclusions have important implications for our understanding of the behavior of middle continental crust during orogenesis.

Block-Type Architecture of Lowermost Middle Continental Crust

The Upper Granite Gorge preserves some of the highest-pressure Paleoproterozoic rocks, and, thus, represents one of the deepest exposures of continental crust in the southwestern United States. This area experienced minimal reheating (~350–500 °C) during ca. 1.5–1.38 Ga tectonometamorphic events (Karlstrom et al., 1997). Consequently, the transect provides a rare window into ca. 1.7 Ga lowermost middle continental crust. The exposure records critical information about the character of the crustal column *beneath* the shallower levels that are now exposed throughout the rest of the Arizona transition zone (Karlstrom and Bowring, 1988; Williams, 1991). The distinctive overprinting of shallow S_1 by steep S_2 domains may be a common style of middle and lower crustal fabric. It imparts a partitioned character to the crust with segmentation at all scales, from a single microlithon (Fig. 8E) to the observed ten-kilometer-scale block-type architecture (Fig. 3). Similar fabric overprinting and the resulting partitioned geometry are also seen in the lower crust of NW Canada (e.g., Mahan and Williams, 2005) and in a variety of crustal levels preserved in Fiordland, New Zealand (e.g., Klepeis et al., 2004).

Rheology of Middle Continental Crust during Orogenesis

Recent contributions have emphasized the potential importance of subhorizontal channel flow in the middle crust during deformation in large, thermally weakened orogens (e.g., Beaumont et al., 2004). Such flow is thought to result from development of an orogenic plateau with steep, marginal topographic gradients (e.g., the Himalayas; Clark and Royden, 2000) and subhorizontal fabric development at depth (e.g., Royden, 1996). In contrast, the view from the middle crust exposed in the Upper Granite Gorge is one characterized by subvertical fabric development during the thermal peak, e.g., the Mineral Canyon block. Although hot blocks in the Upper Granite Gorge were at temperatures on the order of 750 °C where partial melting made the crust weak enough to flow (according to thermal-mechanical numerical models; Beaumont et al., 2004), large-scale horizontal channel flow was apparently inhibited by colder, stronger blocks (e.g., the Topaz Canyon and Clear Creek blocks) that reinforced the block-type architecture. Protracted development of subvertical fabric throughout burial and exhumation of the Upper Granite Gorge may be a record of strain-hardening in a heterogeneous medium undergoing temporally and spatially varying degrees of thermal weakening (see also Karlstrom and Williams, 1998, 2006). Thus, the scale and style of heterogeneity of middle continental crust have a profound impact on the resulting rheological behavior and susceptibility to flow that needs to be considered in future channel flow models.

Exhumation of Orogens, Strain-Hardening, and Preservation of Isobaric Levels of Continental Crust

The *P-T-t-D* path that the middle crust follows during orogeny is directly related to surface erosion (e.g., Jamieson et al., 2004). This has important implications for exhumation of the Upper Granite Gorge, where such a large transect (>70 km long measured perpendicular to S_2) records the same path. Exhumation took place synchronously with development and intensification of subvertical foliation and without evidence for differential uplift or tilting. Decompression of the Upper Granite Gorge transect from ~0.7 to ~0.3–0.4 GPa (~11–14 km) between ca. 1.7 and 1.68 Ga indicates a time-averaged exhumation rate of ~0.55–0.7 mm/yr. These rates are small relative to Phanerozoic orogenic belts like the Coast Mountains of British Columbia (>2.0mm/yr; Hollister, 1982) and the ultrahigh-pressure Dora Maira Unit of the Western Alps (16–34 mm/yr; Rubatto and Hermaan, 2001). We suggest that exhumation was driven by erosion during crustal shortening (e.g., Hollister, 1979), coupled with isostatic adjustments at the scale of the entire transect. Vertical fabric intensification may reflect strain hardening and strengthening of the middle continental crust, a process that would enhance the preservation of near-isobaric sections of continental crust during exhumation.

ACKNOWLEDGMENTS

This study is an outgrowth of over a decade of collaborative, multidisciplinary work on basement rocks in the Grand Canyon. We appreciate the many individuals who have accompanied University of New Mexico research trips and have provided field observations, mapping, and discussions. We acknowledge support from National Science Foundation (NSF) grants EAR-9508096, EAR- 9902955, and EAR-0003477, in addition to support and research permits received from Grand Canyon National Park. We are especially indebted to Sam Bowring, Becky Flowers, Philippe Goncalves, Matt Heizler, and Mike Timmons for numerous discussions regarding the Proterozoic geology of the Southwest. Roger Powell is gratefully acknowledged for his advice regarding the application of the Δ*PT* technique. Our efforts would not have been possible without the outstanding microprobe analytical support of Mike Jercinovic at University of Massachusetts–Amherst. We appreciate the constructive reviews by John Fletcher, Kurt Stüwe, and Associate Editor Ben van der Pluijm.

REFERENCES CITED

Beaumont, C., Jamieson, R.A., Nguyen, M.H., and Medvedev, S., 2004, Crustal channel flows: 1. Numerical models with applications to the tectonics of the Himalayan-Tibetan orogen: Journal of Geophysical Research, v. 109, B06406, doi: 10.1029/2003JB002809.

Bowring, S.A., and Karlstrom, K.E., 1990, Growth and stabilization of Proterozoic lithosphere in the southwestern United States: Geology, v. 18, p. 1203–1206, doi: 10.1130/0091-7613(1990)018<1203:GSAROP>2.3.CO;2.

Cherniak, D.J., 1993, Lead diffusion in titanite and preliminary results on the effects of radiation damage on Pb transport: Chemical Geology, v. 110, p. 177–194, doi: 10.1016/0009-2541(93)90253-F.

Clark, M.K., and Royden, L.H., 2000, Topographic ooze: Building the eastern margin of Tibet by lower crustal flow: Geology, v. 28, no. 8, p. 703–706, doi: 10.1130/0091-7613(2000)028<0703:TOBTEM>2.3.CO;2.

Collins, W.J., and Vernon, R.H., 1991, Orogeny associated with anticlockwise *P-T-t* paths: Evidence from low-*P*, high-*T* metamorphic terranes in the Arunta Inlier, central Australia: Geology, v. 19, no. 8, p. 835–838, doi: 10.1130/0091-7613(1991)019<0835:OAWAPT>2.3.CO;2.

Daniel, C.G., Hollister, L.S., Parrish, R.R., and Grujic, D., 2003, Exhumation of the Main Central thrust from lower crustal depths, eastern Bhutan Himalaya: Journal of Metamorphic Geology, v. 21, no. 4, p. 317–334.

Duebendorfer, E.M., Chamberlain, K.R., and Jones, C.S., 2001, Paleoproterozoic tectonic history of the Cerbat Mountains, northwestern Arizona: Implications for crustal assembly in the southwestern United States: Geological Society of America Bulletin, v. 113, no. 5, p. 575–590, doi: 10.1130/0016-7606(2001)113<0575:PTHOTC>2.0.CO;2.

Dumond, G., Williams, M.L., Mahan, K.H., Karlstrom, K.E., Heizler, M.T., and Jercinovic, M.J., 2004, Tectonic heredity in the Grand Canyon and implications for Tibetan-scale Mesoproterozoic intra-continental deformation in the southwestern United States: Geological Society of America Abstracts with Programs, v. 36, no. 5, p. 403.

Flowers, R.M., Mahan, K.H., Bowring, S.A., Williams, M.L., Pringle, M.S., and Hodges, K.V., 2006, Multistage exhumation and juxtaposition of lower continental crust in the western Canadian Shield: Linking high-resolution U-Pb and ^{40}Ar/^{39}Ar thermochronometry with pressure-temperature-deformation paths: Tectonics, v. 25, TC4003, doi: 10.1029/2005TC001912.

Fraser, G., Worley, B., and Sandiford, M., 2000, High-precision geothermobarometry across the High Himalayan metamorphic sequence, Langtang Valley, Nepal: Journal of Metamorphic Geology, v. 18, p. 665–681, doi: 10.1046/j.1525-1314.2000.00283.x.

Grambling, J.A., 1986, Crustal thickening during Proterozoic metamorphism and deformation in New Mexico: Geology, v. 14, no. 2, p. 149–152, doi: 10.1130/0091-7613(1986)14<149:CTDPMA>2.0.CO;2.

Hawkins, D.P., 1996, U-Pb geochronological constraints on the tectonic and thermal evolution of Paleoproterozoic crust in the Grand Canyon, Arizona [Ph.D. thesis]: Cambridge, Massachusetts Institute of Technology, 320 p.

Hawkins, D.P., and Bowring, S.A., 1999, U-Pb monazite, xenotime, and titanite geochronological constraints on the prograde to post-peak metamorphic thermal history of Paleoproterozoic migmatites from the Grand Canyon, Arizona: Contributions to Mineralogy and Petrology, v. 134, p. 150–169, doi: 10.1007/s004100050475.

Hawkins, D.P., Bowring, S.A., Ilg, B.R., Karlstrom, K.E., and Williams, M.L., 1996, U-Pb geochronological constraints on Paleoproterozoic crustal evolution, Upper Granite Gorge, Grand Canyon, Arizona: Geological Society of America Bulletin, v. 108, p. 1167–1181, doi: 10.1130/0016-7606(1996)108<1167:UPGCOT>2.3.CO;2.

Hodges, K.V., and McKenna, L.W., 1987, Realistic error propagation of uncertainties in geologic thermobarometry: The American Mineralogist, v. 72, p. 671–680.

Holland, T.J.B., and Powell, R., 1998, An internally consistent thermodynamic data set for phases of petrological interest: Journal of Metamorphic Geology, v. 16, p. 309–343, doi: 10.1111/j.1525-1314.1998.00140.x.

Hollister, L.S., 1979, Metamorphism and crustal displacements: New insights: Episodes, v. 3, p. 3–8.

Hollister, L.S., 1982, Metamorphic evidence for rapid (2 mm/yr) uplift of a portion of the Central Gneiss Complex, Coast Mountains, B.C.: Canadian Mineralogist, v. 20, p. 319–332.

Ilg, B.R., and Karlstrom, K.E., 2000, Porphyroblast inclusion trail geometries in the Grand Canyon: Evidence for non-rotation and rotation?: Journal of Structural Geology, v. 22, p. 231–243, doi: 10.1016/S0191-8141(99)00150-9.

Ilg, B.R., Karlstrom, K.E., Williams, M.L., and Hawkins, D.P., 1996, Tectonic evolution of Paleoproterozoic rocks in the Grand Canyon: Insights into middle crustal processes: Geological Society of America Bulletin, v. 108, p. 1149–1166.

Jamieson, R.A., Beaumont, C., Medvedev, S., and Nguyen, M.H., 2004, Crustal channel flows: 2. Numerical models with implications for metamorphism in the Himalayan-Tibetan orogen: Journal of Geophysical Research, v. 109, B06407, doi: 10.1029/2003JB002811.

Johnson, T.E., Brown, M., and Solar, G.S., 2003, Low-pressure subsolidus and suprasolidus phase equlibria in the MnNCKFMASH system: Constraints on conditions of regional metamorphism in western Maine, northern Appalachians: The American Mineralogist, v. 88, p. 624–638.

Karlstrom, K.E., and Bowring, S.A., 1988, Early Proterozoic assembly of tectonostratigraphic terranes in southwestern North America: The Journal of Geology, v. 96, p. 561–576.

Karlstrom, K.E., and Williams, M.L., 1998, Heterogeneity of the middle crust: Implications for strength of continental lithosphere: Geology, v. 26, p. 815–818, doi: 10.1130/0091-7613(1998)026<0815:HOTMCI>2.3.CO;2.

Karlstrom, K.E., and Williams, M.L., 2006, Nature of the middle crust-heterogeneity of structure and process due to pluton-enhanced tectonism: An example from Proterozoic rocks of the North American Southwest, *in* Brown, M., and Rushmer, T., eds., Evolution and Differentiation of the Continental Crust: Cambridge, Cambridge University Press, p. 268–295.

Karlstrom, K.E., Heizler, M.T., and Williams, M.L., 1997, ^{40}Ar-^{39}Ar muscovite thermochronology within the Upper Granite Gorge of the Grand Canyon: Eos, (Transactions, American Geophysical Union), Fall Meeting Supplement, v. 78, no. 46, p. F784.

Karlstrom, K.E., Åhäll, K.I., Harlan, S.S., Williams, M.L., McLelland, J., and Geissman, J.W., 2001, Long-lived (1.8–0.8 Ga) convergent orogen in southern Laurentia, its extensions to Australia and Baltica, and implications for refining Rodinia: Precambrian Research, v. 111, p. 5–30, doi: 10.1016/S0301-9268(01)00154-1.

Karlstrom, K.E., Ilg, B.R., Williams, M.L., Hawkins, D.P., Bowring, S.A., and Seaman, S.J., 2003, Paleoproterozoic rocks of the Granite Gorges, *in* Beus, S.S., and Morales, M., eds., Grand Canyon Geology (2nd ed.): Oxford, Oxford University Press, p. 9–38.

Klepeis, K.A., Clarke, G.L., and Rushmer, T., 2003, Magma transport and coupling between deformation and magmatism in the continental lithosphere: GSA Today, v. 13, no. 1, p. 4–11, doi: 10.1130/1052-5173(2003)013<0004:MTACBD>2.0.CO;2.

Klepeis, K.A., Clarke, G.L., Gehrels, G., and Vervoort, J., 2004, Processes controlling vertical coupling and decoupling between the upper and lower crust of orogens: Results from Fiordland, New Zealand: Journal of Structural Geology, v. 26, p. 765–791, doi: 10.1016/j.jsg.2003.08.012.

Kohn, M.J., 2003, Geochemical zoning in metamorphic minerals, *in* Rudnick, R.L., ed., Treatise on Geochemistry: The Crust: Amsterdam, Elsevier, p. 229–261.

Kohn, M.J., and Spear, F.S., 2000, Retrograde net transfer reaction insurance for pressure- temperature estimates: Geology, v. 28, no. 12, p. 1127–1130, doi: 10.1130/0091-7613(2000)028<1127:RNTRIF>2.3.CO;2.

Kretz, R., 1983, Symbols for rock-forming minerals: The American Mineralogist, v. 68, p. 277–279.

Mahan, K.H., and Williams, M.L., 2005, Reconstruction of a large deep-crustal terrane: Implications for the Snowbird tectonic zone and early growth of Laurentia: Geology, v. 33, p. 385–388, doi: 10.1130/G21273.1.

Percival, J.A., and West, G.F., 1994, The Kapuskasing Uplift—A geological and geophysical synthesis: Canadian Journal of Earth Sciences, v. 31, p. 1256–1286.

Powell, R., and Holland, T.J.B., 1994, Optimal geothermometry and geobarometry: The American Mineralogist, v. 79, p. 120–133.

Pyle, J.M., and Spear, F.S., 1999, Yttrium zoning in garnet: Coupling of major and accessory phases during metamorphic reactions: Geological Materials Research, v. 1, no. 6, p. 1–49.

Royden, L.H., 1996, Coupling and decoupling of crust and mantle in convergent orogens: Implications for strain partitioning in the crust: Journal of Geophysical Research, v. 101, p. 17,679–17,705, doi: 10.1029/96JB00951.

Rubatto, D., and Hermaan, J., 2001, Exhumation as fast as subduction?: Geology, v. 29, no. 1, p. 3–6, doi: 10.1130/0091-7613(2001)029<0003:EAFAS>2.0.CO;2.

Spear, F.S., 1993, Metamorphic Phase Equilibria and Pressure-Temperature-Time Paths: Washington, D.C., Mineralogical Society of America, 799 p.

Spear, F.S., and Cheney, J.T., 1989, A petrogenetic grid for pelitic schists in the system SiO_2- Al_2O_3- FeO-MgO-K_2O-H_2O: Contributions to Mineralogy and Petrology, v. 101, p. 149–164, doi: 10.1007/BF00375302.

Spear, F.S., Selverstone, J., Hickmott, D., Crowley, P., and Hodges, K.V., 1984, *P-T* paths from garnet zoning: A new technique for deciphering tectonic processes in crystalline terranes: Geology, v. 12, p. 87–90, doi: 10.1130/0091-7613(1984)12<87:PPFGZA>2.0.CO;2.

Spear, F.S., Kohn, M.J., Florence, F.P., and Menard, T., 1991, A model for garnet and plagioclase growth in pelitic schists: Implications for thermobarometry and *P-T* path determinations: Journal of Metamorphic Geology, v. 8, p. 683–696.

Spear, F.S., Kohn, M.J., and Cheney, J.T., 1999, *P-T* paths from anatectic pelites: Contributions to Mineralogy and Petrology, v. 134, p. 17–32, doi: 10.1007/s004100050466.

Tenczer, V., and Stüwe, K., 2003, The metamorphic field gradient in the eclogite type locality, Koralpe region, eastern Alps: Journal of Metamorphic Geology, v. 21, no. 4, p. 377–394.

Todd, C.S., and Engi, M., 1997, Metamorphic field gradients in the central Alps: Journal of Metamorphic Geology, v. 15, no. 4, p. 513–530, doi: 10.1111/j.1525-1314.1997.00038.x.

Whitney, D.L., and Dilek, Y., 1998, Characterization and interpretation of *P-T* paths with multiple thermal peaks, *in* Treloar, P.J., and O'Brien, P.J., eds., What Drives Metamorphism and Metamorphic Reactions?: Geological Society of London Special Publication 138, p. 53–60.

Williams, M.L., 1991, Overview of Proterozoic metamorphism in Arizona, *in* Karlstrom, K.E., ed., Proterozoic Geology and Ore Deposits of Arizona: Arizona Geological Society Digest, v. 19, p. 11–26.

Williams, M.L., and Jercinovic, M.J., 2002, Microprobe monazite geochronology: Putting absolute time into microstructural analysis: Journal of Structural Geology, v. 24, p. 1013–1028, doi: 10.1016/S0191-8141(01)00088-8.

Williams, M.L., and Karlstrom, K.E., 1996, Looping *P-T* paths and high-*T*, low-*P* middle crustal metamorphism: Proterozoic evolution of the southwestern United States: Geology, v. 24, no. 12, p. 1119–1122, doi: 10.1130/0091-7613(1996)024<1119:LPTPAH>2.3.CO;2.

Worley, B., and Powell, R., 2000, High-precision relative thermobarometry: Theory and worked example: Journal of Metamorphic Geology, v. 18, p. 91–101, doi: 10.1046/j.1525-1314.2000.00239.x.

Manuscript Received 25 September 2005
Revised Manuscript Received 25 July 2006
Manuscript Accepted 2 August 2006

Printed in the USA